Anti-oncostatin M antibody inhibits the pro-malignant effects of oncostatin M receptor over-expression in squamous cell carcinoma

Justyna A Kucia-Tran[1], Valtteri Tulkki[1], Cinzia G Scarpini[1], Stephen Smith[1], Maja Wallberg[1], Marta Paez-Ribes[1], Angela M Araujo[2], Jan Botthoff[1], Maria Feeney[3], Katherine Hughes[4], Maria M Caffarel[1,2,5,*], Nicholas Coleman[1,*]

[1] Department of Pathology, University of Cambridge, Cambridge, United Kingdom

[2] Biodonostia Research Institute, San Sebastian, Spain

[3] GlaxoSmithKline, Stevenage, United Kingdom

[4] Department of Veterinary Medicine, University of Cambridge, Cambridge, United Kingdom

[5] IKERBASQUE, Basque Foundation for Science, Bilbao, Spain

***Correspondence to**: Prof. Nicholas Coleman, Department of Pathology, University of Cambridge, Tennis Court Road, Cambridge, CB2 1QP, UK, E-mail: nc109@cam.ac.uk, Tel: +44-1223766422; Fax: +44-1223333346 or Dr. Maria M. Caffarel, Biodonostia Research Institute, San Sebastian, 20014, Spain and IKERBASQUE, Basque Foundation for Science, Bilbao, 48013, Spain, Email: maria.caffarel@biodonostia.org, Tel: +34-943006296.

Competing interests: The authors declare no conflicts of interest.

Running head: OSMR signalling and effects of anti-OSM antibody in squamous cell carcinoma

Word count: 3994

Abstract

The oncostatin M receptor (OSMR) shows frequent gene copy-number gain and over-expression in cervical squamous cell carcinomas (SCCs), associated with adverse clinical outcomes. In SCC cells that overexpress OSMR, the major ligand OSM induces multiple pro-malignant effects, including invasion, secretion of angiogenic factors and metastasis. Here we demonstrate, for the first time, that OSMR over-expression in SCC cells activates cell-autonomous feed-forward signalling, via further expression of OSMR and OSM and sustained STAT3 activation despite expression of the negative regulator SOCS3. The pro-malignant effects associated with OSMR overexpression are critically mediated by JAK/STAT3 activation, which is induced by exogenous OSM and also by autocrine OSM:OSMR interactions. Importantly, specific inhibition of OSM:OSMR interactions by neutralizing antibodies significantly inhibits STAT3 activation and feed-forward signalling, leading to reduced invasion, angiogenesis and metastasis. Our findings are supported by data from 1,254 clinical SCC samples, in which OSMR levels correlated with multiple cognate genes, including OSM, STAT3 and downstream targets. These data strongly support the development of OSM:OSMR blocking antibodies as biologically targeted therapies against SCCs of the cervix and other anatomical sites.

Keywords: Cervix, head and neck, squamous cell carcinoma, oncostatin M receptor, neutralizing antibodies, metastasis, STAT3.

Introduction

Many of the common human malignancies are squamous cell carcinomas (SCCs), in which tumour cells show features of squamous cell (keratinocyte) differentiation. High-risk human papillomavirus (HR-HPV) is a definite carcinogen for SCCs at multiple sites, including the cervix and head/neck [1]. Cervical carcinoma causes ~300,000 deaths p.a., while incidence rates of head/neck SCCs are rising rapidly [2]. There is an important need for new treatments in SCC and the recent success of antibody-based approaches in improving overall survival [3, 4] has strengthened the case for developing novel targeted therapies.

Previous work has identified the oncostatin M receptor (OSMR) as a cell surface target suitable for antibody inhibition in cervical and other SCCs [5-7]. The *OSMR* gene is located on chromosome 5p, a genomic region that showed one of the highest rates of copy number gain in advanced cervical SCCs [8]. *OSMR* gain was seen in >60% of cervical SCCs (n=146 total) and was associated with significantly worse overall survival, producing a relative risk of death of 3.6 [8]. There was a significant correlation between *OSMR* gene copy number and *OSMR* transcript levels [9]. Importantly, high levels of OSMR associated with highly significant adverse overall survival in 251 cervical SCCs from The Cancer Genome Atlas (TCGA) (p=0.006) [9]. OSMR was also over-expressed in SCCs from multiple additional sites, including head/neck, skin and vulva [9], as well as in other common malignancies. The latter included breast adenocarcinoma [10], where high levels were associated with adverse clinical outcomes, and glioblastoma multiforme [11, 12].

OSMR is one of a group of receptors for cytokines of the interleukin-6 (IL6) family [13, 14]. It associates with gp130 to form a heterodimer that binds the major ligand oncostatin M (OSM) and also with gp130-like (GPL) protein to form a heterodimeric receptor for interleukin-31 (IL31). Human OSM (but not murine OSM) can also bind heterodimers of gp130 and leukemia inhibitory factor

receptor (LIFR), another IL6-family cytokine receptor [15]. OSM:OSMR interactions can activate multiple signalling pathways, leading to the transcription of a wide range of context-dependent target genes [14, 16]. We previously showed that OSM treatment of OSMR over-expressing cervical SCC cells exerted pro-malignant effects, including *in vitro* induction of cell migration/invasion, epithelial to mesenchymal transition (EMT) and secretion of pro-angiogenic factors; as well as increased experimental lung metastasis *in vivo* [5, 6, 9]. Key mediators of the observed effects included VEGFA, transglutaminase-2 (TGM2) and several EMT transcription factors, e.g. *SNAI1* [5, 6, 9]. *In vivo*, OSM is secreted by a variety of cell types in the tumour microenvironment, particularly macrophages and dendritic cells [13, 14].

In the present study, we dissected which signalling pathways mediated the multiple pro-malignant effects of OSM:OSMR interactions in SCC cells from the cervix and other sites, in order to determine the most rational strategies for therapeutic inhibition. Our data strongly support the development of OSM:OSMR blocking antibodies as biologically-targeted therapies against SCCs of the cervix and other anatomical sites.

Materials and Methods

Cell culture

The SCC cell lines used are listed in supplementary information, Table S1. For control samples, we used primary cultures of normal ectocervical epithelium (NCx6, NCx95, NCx96) from three hysterectomy specimens removed for non-neoplastic disease unrelated to the cervix [8]. The SCC cell lines selected for detailed *in vitro* analysis (CaSki, SW756, ME180, MS751, OSC19 and HSC1) were authenticated by short tandem repeat profiling (ATCC-LGC, Middlesex, UK).

Recombinant human OSM (R&D Systems, Minneapolis, MN, USA) was added to cells at 10 ng/ml, in keeping with previous studies examining the effects of OSM in tissue culture [5, 17, 18]. For OSM pulse treatment, OSM was added for 15 min and cells washed twice with PBS before new medium was added. Recombinant human LIF and IL6 (R&D Systems) were used at up to 100 and 400 ng/ml, respectively. Secretion of OSM and IL6 was measured using human OSM DuoSet ELISA (R&D Systems) and Mini TMB ELISA (PeproTech, Rocky Hill, NJ, USA), respectively, normalizing for cell number. To neutralize exogenous OSM *in vitro* and *in vivo*, cells were treated with 0.25 µg/ml humanized IgG1 monoclonal anti-OSM antibody GSK2330811 (GlaxoSmithKline Stevenage, UK), unless otherwise specified, for 1 h prior to OSM treatment. To neutralize endogenous production of OSM and IL6, cells were pulsed for 15 min with OSM, washed twice with PBS, then treated with up to 1 µg/ml GlaxoSmithKline humanized anti-OSM antibody or 2.5 µg/ml anti-IL6 antibody (#500-P26, PeproTech) for between 1 and 24 h. Equal volumes of PBS (vehicle) or equal concentrations of a control humanized IgG antibody (Synagis, MedImmune, Cambridge, UK) were added to the cells as controls.

For signalling pathway inhibition, cells were pre-treated for 2 h with medium supplemented with TG101348 (Axon Medchem BV, Groningen, The Netherlands), Ruxolitinib (InvivoGen, Toulouse, France), S3I-201 (Sigma-Aldrich, St. Louis, USA), Stattic (Cayman Chemical Company, Ann Arbor, MI, USA), LY294002 HCl (StressMarq Biosciences Inc., Victoria, Canada), PD98059 (Cell Signaling Technology, Danvers, USA) or PP242 (Cayman Chemical Company). For each molecule, we chose the lowest concentration that inhibited the target pathway in SW756 cells and also caused no significant cytotoxicity *in vitro*. Control cells were treated with equivalent volumes of PBS or DMSO vehicle (vol/vol) only. Cell viability was assessed using an MTT assay (Sigma-Aldrich).

Cell transfections

For gene depletion, the targets *OSMR*, *LIFR* and *STAT3* were each depleted using a 40 nM pool of four siRNAs (ON-TARGETplus SMARTpool L-008050, L-008017, L-003544, respectively; Dharmacon, Lafayette, LA, USA) and compared with cells treated with pooled non-targeting control (NTC) siRNAs (ON-TARGETplus Non-targeting Pool, D-001810-10-05, Dharmacon), as described [19]. OSM or PBS was added 24 h after transfection and cells were treated for a further 24 or 48 h. siRNA sequences are given in supplementary material, Table S2.

To over-express OSMR, ME180 and MS751 cells were transiently transfected with 0.5 or 1 µg, respectively, of pcDNA3.1zeo-hOSMR plasmid [5]. Control transfections used an equivalent amount of empty pcDNA3.1zeo vector. For OSM over-expression, SW756 cells were stably transfected with 2 µg of pUNO1-hOSM expression construct (InvivoGen). Control transfections used 2 µg of pUNO1-mcs control vector. For *in vivo* experiments, bioluminescent SW756 cells were generated by stable transfection of pGL4.51 luciferase reporter vector (Promega, Southampton, UK).

RT-qPCR, Western blotting, cell invasion and angiogenesis assays

Relative mRNA and DNA levels were measured using qPCRBIO SyGreen Mix (PCR Biosystems, London, UK) (supplementary material, Table S3). Reverse transcription was done using 1 µg total RNA and QuantiTect Reverse Transcription (Qiagen, Crawley, UK). Expression ratios were calculated using the comparative threshold cycle method [20], normalizing to three reference genes: *HMBS*, *YWHAZ* and *RPL13A* [21]. DNA ratios were normalized to the *ACTB* promoter, *GAPDH* promoter and myoglobin promoter. They were referenced to normal cervix tissue (NCx6), in which there was one copy of the *OSMR* gene per haploid genome. Copy number gain of *OSMR* was defined by DNA levels at least two-fold greater than the mean for NCx6. Western blotting was performed as described [6], using the antibodies listed in supplementary material, Table S4. Details of the cell invasion and angiogenesis assays are given in supplementary material, Materials and methods.

***In vivo* experimental metastasis**

Bioluminescent SW756 cells (1 x 10^6 in 200 µl), subjected to different treatments, were injected into the lateral tail vein of 5–6-week old female NOD SCID (NOD.CB17-*Prkdcscid*/NcrCrl) mice (Charles River, Oxford, UK), using 29-gauge insulin needles. Growth of lung tumours was monitored non-invasively using the Living Image 3.2 In Vivo Imaging Software (PerkinElmer, Waltham, MA, USA). Initial measurements were made 30 min after tail vein injection, to confirm equal cell access to the lungs, followed by serial whole-body imaging at weekly intervals. All mice were maintained in conventional cages within a specific pathogen-free animal facility. They were treated in strict accordance with guidelines from the Cambridge University Licence Review Committee and the UK Home Office. The data obtained using the In Vivo Imaging Software were confirmed by two independent methods, namely histology and qPCR measurement of human DNA levels in the mouse lung tissue at the end of the experiment. Details are given in supplementary material, Materials and methods.

Bioinformatics and statistical analysis

We analysed mRNA levels of *OSMR*, *EGFR*, *VEGFA*, *TGM2*, *OSM* and *STAT3* in the publically-available next-generation sequencing data of The Cancer Genome Atlas. Details of the bioinformatics used and the statistical analyses performed are given in Supplementary material, Materials and methods.

Results

OSMR over-expression in SCC cells enhances responsiveness to OSM

We first compared signalling responses to OSM pulse-stimulation in two SCC cell lines from the same tissue of origin (cervix) that had high or low levels of OSMR protein (SW756 and ME180, respectively) (supplementary material, Figure S1). Following pulsed OSM exposure (10 ng/ml for 15 min) (supplementary material, Figure S2A), activated STAT3, STAT5, AKT and ERK1/2 were induced at higher signal intensity and for a longer duration in the OSMR high cells (SW756), compared with the OSMR low cells (ME180) (Figure 1A-B and supplementary material, Figure S2B). The SW756 cells showed very rapid and sustained activation of STAT3, which was detectable 15 min after the OSM pulse and lasted for up to 72 h. The intensity and duration of induction of total EGFR (which has recently been shown to contribute to OSMR signalling [12]), and STAT1 were also greater in SW756 than in ME180, although there were no differences in levels of induction of the activated (phosphorylated) forms (Figure 1A-B). Despite its effects on total EGFR protein, OSM did not alter *EGFR* transcript levels in SW756 cells after 24 or 48 h of continuous treatment (supplementary material,Figure S2C). STAT3 was also rapidly activated by pulsed OSM treatment in head/neck and skin SCC cells identified as expressing high levels of OSMR (OSC19 and HSC1, respectively) (supplementary material, Figures S1 and S2D-E). The enhanced and sustained activation of STAT3 and ERK in OSMR-high cervical SCC cells was also confirmed in two additional cell lines: CaSki and MS751, which show high and low OSMR levels respectively (supplementary material, Figure S1 and supplementary material, Figure S2F).

For two SCC cell lines with low basal OSMR levels (ME180 and MS751), in which OSMR levels had been increased following transient transfection, phosphorylated STAT3 and phosphorylated ERK1/2 were expressed at higher basal levels and showed increased intensity and duration of induction by

pulsed OSM (Figure 1C-D). In SW756 cells, activation of STAT3, STAT5, AKT and ERK1/2 by OSM was abrogated by depleting OSMR but not by depleting LIFR (Figure 1E and supplementary material, Fig S2L-M), indicating that OSM was acting solely through the over-expressed OSMR in these cells. LIFR is functional in SW756, as treatment with LIF induced STAT3 activation (supplementary material, Fig S2G). Interestingly, in low OSMR expressing ME180 cells, activation of STAT3 was partially abrogated by depleting LIFR but not by depleting OSMR (supplementary material, Figure S2H-I).

In keeping with the differences in signalling pathway activation, we observed that genes previously shown to mediate OSM effects in OSMR-over-expressing SCC cells were only induced in the OSMR-over-expressing cells (SW756 and CaSki) and not in cells without OSMR over-expression (MS751 and ME180) (Figure 2A). The genes tested were known mediators of OSM-induced invasion (*TGM2*), EMT (*SNAI1*), and the pro-angiogenic phenotype (*VEGFA*) [5, 6, 9]. All three genes were also induced in head/neck and skin SCC cells with high levels of OSMR (OSC19 and HSC1, respectively) (supplementary material, Figure 2J-K). Forced OSMR over-expression in MS751 following transient transfection was associated with significantly greater induction of all three genes by OSM (Figure 2B). In all four OSMR over-expressing cell lines tested (SW756, CaSki, OSC19 and HSC1), activation of all three genes by OSM was reduced by depleting OSMR but not by depleting LIFR (Figure 2C-D and supplementary material, Figure S2L-M).

JAK2 and STAT3 mediate the pro-malignant effects of OSM:OSMR interactions

We used small molecule inhibitors and siRNAs to identify which of the multiple signalling pathways induced by OSM in OSMR over-expressing SCC cells were responsible for the pro-malignant effects observed (Figure 3 and supplementary material, Figure S3). In SW756, OSM induction of the pro-malignant target genes *VEGFA*, *SNAI1* and *TGM2* was significantly reduced by each of two JAK inhibitors, ruxolitinib (JAK1 and JAK2 inhibitor) and TG101348 (selective JAK2 inhibitor) (Figure 3A-B

and supplementary material, Figure S3A-E). No significant effect on OSM induction of target genes was seen by inhibiting the ERK1/2 pathway with MEK inhibitor PD98059, or by inhibiting mTOR complex 1/2 with PP242. Inhibition of pAKT with PI3K inhibitor LY294002 reduced *VEGFA* basal levels and partially abrogated its induction by OSM. However, there were no significant effects on *SNAI1* and *TGM2*. In SW756 cells transfected to produce OSM constitutively (SW756-pOSM), both JAK inhibitors significantly reduced expression of all three OSMR target genes (Figure 3C and supplementary material, Figure S3F-G).

Specific inhibition of the downstream JAK target STAT3 could not be achieved using small molecule inhibitors, as these also inhibited STAT5 (Supplementary Figure S3H-I). STAT3 depletion using siRNAs (supplementary material, Figure S3J-N) led to significant inhibition of OSM induction of pro-malignant target genes in SW756, CaSki (both Figure 3D), OSC19 and HSC1 cells (both Figure 3E). In keeping with these observations, STAT3 depletion significantly inhibited the increased invasiveness induced by OSM in SW756 cells (Figure 3F).

In SW756 cells treated with non-targeting control siRNAs (siNTC), OSM pre-treatment for 48 h induced a significant increase in lung colonization following tail vein injection, compared with PBS-treated cells (Figure 3G-H and supplementary material, Figure S3O-R). In contrast, SW756 cells treated with STAT3 siRNA (siSTAT3) showed reduced lung colonization following OSM treatment. Interestingly, siSTAT3-treated SW756 cells also showed reduced lung colonization in the absence of OSM pre-treatment, compared with siNTC-treated SW756 cells in the absence of OSM pre-treatment (Figure 3G-H). There were no histological differences in cell morphology or mitotic rate between the lung metastases seen in the different experimental groups.

OSM induces a feed-forward loop in SCC cells, which prolongs STAT3 activation

We examined the kinetics of STAT3 phosphorylation responses at early time points following OSM pulse-stimulation of OSMR-overexpressing SCC cells (SW756). Strong induction was seen after 30 min, followed by induction of SOCS3 (an inhibitor of STAT3 activation) and concurrent reduction in STAT3 phosphorylation by 2 h (Figure 4A). In addition, we consistently observed a second wave of STAT3 activation, approximately 4 h following OSM pulse treatment, despite the presence of SOCS3 (Figures 1A-B and 4A). In OSM-pulsed SCC cells without OSMR over-expression (ME180), this STAT3 reactivation was also detectable but was weaker and delayed (Figure 1A-B).

The re-phosphorylation of STAT3 in the SW756 cells was blocked by inhibiting Golgi transport with monensin (Golgi-STOP) (Figure 4B), indicating a requirement for newly secreted proteins. We hypothesized that such proteins were IL6 family cytokines, which are strong inducers of STAT3 phosphorylation [22]. OSM-pulsed SW756 cells secreted both OSM and IL6 over a 4 h period (Figure 4C-D). Levels of *OSM* mRNA also increased, indicating *de novo* synthesis (Figure 4E). For both ME180 and MS751 cells, cells transfected with OSMR and pulsed with OSM showed greater secretion of OSM over the following 4 h than OSM-pulsed wild-type cells (Figure 4F). However, we could not detect secretion of IL6 by these cells in any of the conditions tested.

In both SW756 and ME180 cells, OSM pulse-stimulation also induced further expression of OSMR, which was detectable after 2–4 h and sustained for at least 72 h (Figure 4G-H). The induction of OSMR was stronger and more prolonged in the cells with baseline OSMR over-expression (SW756), compared with cells without baseline OSMR over-expression (ME180). In keeping with these observations, SW756 cells that constitutively over-expressed OSM following transfection (SW756-pOSM) showed higher *OSMR* mRNA levels than wild-type SW756 cells (Figure 4I).

In SW756 cells treated with a 15 min pulse of OSM (followed by OSM removal), the second wave of STAT3 activation at 4 h was inhibited by anti-OSM neutralizing antibody but not by anti-IL6

neutralizing antibody (Figure 4J and supplementary material, S4A). Inhibition of the second wave of STAT3 activation by the anti-OSM neutralizing antibody persisted to 24 h after the OSM pulse and was accompanied by inhibition of OSMR induction at 4 hours post-pulse (Figure 4K). In keeping with the findings using the anti-IL6 antibody, treatment of SW756 cells with exogenous IL6 (at doses between 100 and 400 ng/ml) did not induce STAT3 activation or expression of pro-malignant target genes (supplementary material, Figure S4B-C), indicating poor sensitivity of these cells to IL6. IL6R mRNA expression in SW756 was low and did not change after OSM treatment (supplementary material, Figure S4D). Unlike OSMR, IL6R (and LIFR) were not over-expressed in SCCs from multiple anatomical sites (supplementary material, Figure S5). In SW756 cells that had not been treated with OSM, the background levels of activated STAT3 were low but detectable after prolonged Western blot exposure (supplementary material, Figure S4E). Treatment of such cells with the anti-OSM neutralising antibody produced a small but discernible reduction in activated STAT3 at 24 h (supplementary material, Figure S4E).

Anti-OSM neutralizing antibody inhibits OSM:OSMR pro-malignant signalling in SCC cells

Together, the above data demonstrated a cell-autonomous feed-forward loop activated by OSM that induced both OSM and OSMR, thereby propagating STAT3 activation. They indicated that anti-OSM neutralizing antibodies would act on OSMR-overexpressing cervical SCC cells at multiple stages in the response to OSM, by inhibiting both the initial effects of OSM exposure and the consequent feed-forward loop, thereby providing sustained suppression of OSM-induced pro-malignant effects. We therefore tested the effect of anti-OSM neutralizing antibodies on the expression of OSMR targets and in functional assays of angiogenesis, invasion and lung colonization (Figure 5).

Anti-OSM neutralizing antibody showed dose-dependent inhibition of OSM activation of OSMR target genes (*VEGFA*, *SNAI1* and *TGM2*) in the OSMR over-expressing cervical SCC cells SW756 and

CaSki (Figure 5 A-B). Whereas conditioned medium from SW756 cells treated with OSM induced endothelial tubule formation in an *in vitro* angiogenesis assay (previously shown to be due to VEGFA secretion [5]), conditioned medium from SW756 cells also treated with anti-OSM neutralizing antibody produced significantly less angiogenesis, as measured by the total length of endothelial cell tubules and the number of tubule junctions formed (Figure 5C-E). In SW756 cells treated with PBS rather than OSM, the anti-OSM neutralizing antibody again reduced tubule length and junction number, although the differences did not reach statistical significance (Figure 5D-E). Furthermore, anti-OSM neutralizing antibody inhibited the increased invasiveness induced by OSM in both SW756 and OSC19 SCC cells (Figure 5F-G). In SW756, the antibody also significantly reduced invasiveness in the absence of exogenous OSM.

In vivo, pre-treatment of luciferase-expressing SW756 cells with the murine 'parental' version of the anti-OSM neutralizing antibody prior to addition of exogenous OSM resulted in significant reduction of lung colonization following tail-vein injection, compared with cells pre-treated with IgG control prior to OSM (Figure 5H-I, compare purple and red lines, p=0.017; supplementary material, Figure S6A-D). In addition, pre-treatment with the anti-OSM neutralizing antibody also significantly reduced lung colonization in the absence of any exogenous OSM, compared with cells pre-treated with IgG control only (Figure 5H-I, compare green and blue lines, and supplementary material, Figure S6E; p = 0.011). The lung colonisation data obtained by the In Vivo Imaging Software were confirmed using two independent methods: histological quantification of the area of lung tissue occupied by malignant cells (supplementary material, Figure S6F) and q-PCR quantification of the amount of human DNA in lung tissue, normalised to 45S ribosomal DNA (Supplementary material, Figure S6G). There were no histological differences in cell morphology or mitotic rate between the lung metastases in the different experimental groups.

OSMR levels correlate with multiple signalling and downstream genes in SCC clinical samples

To test whether our findings were relevant in SCC clinical samples, we examined data from 1,254 SCCs in TCGA. Across SCCs from cervix (n=251), head/neck (n=504) and lung (n=499), *OSMR* mRNA levels showed strong positive correlations with those of *OSM*, *STAT3*, *EGFR* and the downstream genes *VEGFA* and *TGM2* (supplementary material, Figure S7 and Table 1). These observations were supported by previous evidence of an association between levels of *OSMR* and *SNAI1* in the same datasets and an association between OSMR and decreased overall survival in the cervical SCCs [9].

Discussion

Here we have performed the first detailed characterisation of the signalling pathways activated by OSM in SCC cells with OSMR over-expression. We show that the signals induced by exogenous OSM are mediated by OSMR and not by LIFR. We also obtained multiple lines of evidence indicating that OSMR over-expression produces pro-malignant effects in the absence of exogenous OSM. Forced expression of OSMR in cervical SCC cells with low baseline levels (ME180 and MS751) led to increased levels of pSTAT3 and pERK1/2 in the absence of exogenous OSM. Moreover, anti-OSM blocking antibodies reduced invasiveness and experimental lung metastasis in SW756 cells that had not been treated with OSM. Such effects could not be attributed to cross-reactivity with the murine system, as mouse OSM does not bind human OSMR [14] and is not inhibited by the anti-OSM neutralizing antibody used (unpublished data). In keeping with these findings, OSM was detectable in OSM-untreated SW756 cells, at both the mRNA (Figure 4E, first column) and protein levels (0.2 pg/5x10^6 cells; supplementary material, Figure S3F). In addition, treatment with anti-OSM neutralizing antibody inhibited basal STAT3 activation in unstimulated SW756 cells (supplementary material, Figure S4E). Together, these observations indicate functionally significant autocrine OSM:OSMR interactions in SCC cells that over-express OSMR.

We identified that JAKs and STAT3 were critical in inducing all the functionally significant pro-malignant target genes previously shown to be downstream of OSM:OSMR interactions in OSMR over-expressing SCC cells [5, 6, 9]. STAT3 also had an important role in SCC cell experimental lung metastasis, which was significantly reduced following STAT3 depletion, with or without exogenous OSM treatment. Importantly, we also observed a second wave of STAT3 activation following OSM stimulation, due to a novel feed-forward mechanism involving further induction of both OSM and OSMR. This is, to our knowledge, the first evidence that endogenously produced OSM released by cancer cells in response to OSMR-STAT3 activation contributes to the pro-malignant phenotype.

The OSM-dependent STAT3 re-phosphorylation occurred in the presence of the negative regulator SOCS3, indicating the involvement of further STAT3 activating mechanisms that were unaffected by SOCS3. Such mechanisms may involve EGFR, as responses to IL6 in colonic adenocarcinoma cells included a second wave of STAT3 reactivation that was not inhibited by SOCS3, due to direct interactions between IL6R and EGFR [23]. As OSMR is also a receptor for cytokines in the IL6 family, it may serve analogous roles to IL6R in other malignancies, including SCCs. Indeed, it was recently shown that OSMR binds the most common form of mutant EGFR in glioblastoma multiforme cells, to produce a co-receptor that is required for STAT3 signalling [12]. In keeping with these findings, we observed a strong correlation between levels of *OSMR* and *EGFR* transcripts in SCC samples from multiple anatomical sites. Moreover, OSM rapidly increased levels of EGFR protein in cervical SCC cells without affecting transcript levels, supporting a further role for OSMR in increasing EGFR protein stability.

Based on our *in vitro* observations, we reasoned that effective antibody blockade of cell surface OSM:OSMR interactions would inhibit both the initial effects of exogenous OSM and the consequences of feed-forward induction of further OSM and OSMR. In keeping with this prediction, anti-OSM blocking antibodies produced potent anti-malignant effects, both in the presence and absence of exogenous OSM. Ours is the first demonstration that these antibodies inhibit metastasis in relevant pre-clinical animal models. They extend previous evidence that anti-OSM blocking antibodies, including those used here, inhibit the paracrine effects of OSM released by carcinoma-associated adipose tissue on breast adenocarcinoma cells [24]. The anti-OSM neutralizing antibody used in our experiments is safe and well tolerated in man and is presently under clinical evaluation as a therapy for systemic sclerosis and scleroderma [25] (https://clinicaltrials.gov/ct2/show/NCT02386436; https://clinicaltrials.gov/ct2/show/NCT03041025).

In conclusion, improved understanding of the biology of OSMR has indicated its importance as a driver of several common cancers. As a major activator of STAT3 signalling it offers the potential for therapeutic combination with a variety of conventional and targeted agents in current clinical use. We hypothesize that OSM:OSMR blocking antibodies could show clinical benefit in cervical SCCs with OSMR over-expression, which is seen in approximately 50% of advanced cases [9]. Further pre-clinical investigation of the effects of OSM:OSMR blocking antibodies as single agents or in combination therapies for SCC is now strongly indicated. Such work should include immunocompetent mouse models, in which OSM:OSMR effects on local and systemic immune responses can be studied.

Acknowledgments and Funding

This work was funded by Cancer Research UK (Programme Grant A13080) and the Biotechnology and Biological Sciences Research Council Doctoral Training Partnership (grant reference 1221076). MMC acknowledges support from IKERBASQUE Basque Foundation for Science, Spanish Ministry of Economy and Competitiveness (PI15/00623), and European Regional Development (FEDER) funds. KH's research is currently supported by the Isaac Newton/ University of Cambridge/ Wellcome Trust Institutional Strategic Support Fund. We are grateful to Professor Salvador Aznar Benitah (Institute for Research in Biomedicine, The Barcelona Institute of Science and Technology, Spain), Dr. Phil Jones (MRC Cancer Unit, University of Cambridge, UK), Professor Miguel Quintanilla (Universidad Autónoma de Madrid, Spain), Dr. Jane Sterling (Department of Pathology, University of Cambridge, UK) and Professor Fiona Watt (Centre for Stem Cells and Regenerative Medicine, King's College London, UK) for providing SCC cell lines. We thank Professor Tony Green (Department of Haematology, University of Cambridge, UK) for providing TG101348; Professor Christine Watson (Department of Pathology, University of Cambridge, UK) for providing ruxolitinib, S3I-201 and anti-SOCS3 antibody and Mrs. Dawn Ward (Department of Pathology, University of Cambridge, UK) for assistance with cell culture.

Author contributions statement

JKT, MMC and NC designed the study. JKT, VT, CGS, MPR, AMA, JB and MMC performed experiments. MF provided the OSM neutralizing antibody and contributed to experimental design. SS performed the bioinformatics analysis of the TCGA data. MW contributed to the animal experiments. KH analysed the mouse histopathology. JKT, CGS, MMC and NC analysed the data and wrote the manuscript. All authors had final approval of the submitted and published versions.

References

1. Groves IJ, Coleman N. Pathogenesis of human papillomavirus-associated mucosal disease. *J Pathol* 2015; **235**: 527-538.
2. Ferlay J, Soerjomataram I, Dikshit R*, et al.* Cancer incidence and mortality worldwide: sources, methods and major patterns in GLOBOCAN 2012. *Int J Cancer* 2015; **136**: E359-386.
3. Tewari KS, Monk BJ. New strategies in advanced cervical cancer: from angiogenesis blockade to immunotherapy. *Clin Cancer Res* 2014; **20**: 5349-5358.
4. Fung C, Grandis JR. Emerging drugs to treat squamous cell carcinomas of the head and neck. *Expert Opin Emerg Drugs* 2010; **15**: 355-373.
5. Winder DM, Chattopadhyay A, Muralidhar B*, et al.* Overexpression of the oncostatin M receptor in cervical squamous cell carcinoma cells is associated with a pro-angiogenic phenotype and increased cell motility and invasiveness. *J Pathol* 2011; **225**: 448-462.
6. Caffarel MM, Chattopadhyay A, Araujo AM*, et al.* Tissue transglutaminase mediates the pro-malignant effects of oncostatin M receptor over-expression in cervical squamous cell carcinoma. *J Pathol* 2013; **231**: 168-179.
7. Caffarel MM, Coleman N. Oncostatin M receptor is a novel therapeutic target in cervical squamous cell carcinoma. *J Pathol* 2014; **232**: 386-390.
8. Ng G, Winder D, Muralidhar B*, et al.* Gain and overexpression of the oncostatin M receptor occur frequently in cervical squamous cell carcinoma and are associated with adverse clinical outcome. *J Pathol* 2007; **212**: 325-334.
9. Kucia-Tran JA, Tulkki V, Smith S*, et al.* Overexpression of the oncostatin-M receptor in cervical squamous cell carcinoma is associated with epithelial-mesenchymal transition and poor overall survival. *Br J Cancer* 2016; **115**: 212-222.
10. West NR, Murphy LC, Watson PH. Oncostatin M suppresses oestrogen receptor-alpha expression and is associated with poor outcome in human breast cancer. *Endocr Relat Cancer* 2012; **19**: 181-195.
11. Natesh K, Bhosale D, Desai A*, et al.* Oncostatin-M differentially regulates mesenchymal and proneural signature genes in gliomas via STAT3 signalling. *Neoplasia* 2015; **17**: 225-237.
12. Jahani-Asl A, Yin H, Soleimani VD*, et al.* Control of glioblastoma tumorigenesis by feed-forward cytokine signaling. *Nat Neurosci* 2016; **19**: 798-806.
13. Tanaka M, Miyajima A. Oncostatin M, a multifunctional cytokine. *Rev Physiol Biochem Pharmacol* 2003; **149**: 39-52.
14. Hermanns HM. Oncostatin M and interleukin-31: Cytokines, receptors, signal transduction and physiology. *Cytokine Growth Factor Rev* 2015; **26**: 545-558.
15. Drechsler J, Grotzinger J, Hermanns HM. Characterization of the rat oncostatin M receptor complex which resembles the human, but differs from the murine cytokine receptor. *PLoS One* 2012; **7**: e43155.
16. Richards CD. The enigmatic cytokine oncostatin m and roles in disease. *ISRN Inflamm* 2013; **2013**: 512103.
17. Wijelath ES, Carlsen B, Cole T*, et al.* Oncostatin M induces basic fibroblast growth factor expression in endothelial cells and promotes endothelial cell proliferation, migration and spindle morphology. *J Cell Sci* 1997; **110 (Pt 7)**: 871-879.
18. Cawston T, Billington C, Cleaver C*, et al.* The regulation of MMPs and TIMPs in cartilage turnover. *Ann N Y Acad Sci* 1999; **878**: 120-129.
19. Hanning JE, Saini HK, Murray MJ*, et al.* Lack of correlation between predicted and actual off-target effects of short-interfering RNAs targeting the human papillomavirus type 16 E7 oncogene. *Br J Cancer* 2013; **108**: 450-460.
20. Pfaffl MW. A new mathematical model for relative quantification in real-time RT-PCR. *Nucleic Acids Res* 2001; **29**: e45.

21. Vandesompele J, De Preter K, Pattyn F*, et al.* Accurate normalization of real-time quantitative RT-PCR data by geometric averaging of multiple internal control genes. *Genome Biol* 2002; **3**: RESEARCH0034.
22. Yu H, Lee H, Herrmann A*, et al.* Revisiting STAT3 signalling in cancer: new and unexpected biological functions. *Nat Rev Cancer* 2014; **14**: 736-746.
23. Wang Y, van Boxel-Dezaire AH, Cheon H*, et al.* STAT3 activation in response to IL-6 is prolonged by the binding of IL-6 receptor to EGF receptor. *Proc Natl Acad Sci U S A* 2013; **110**: 16975-16980.
24. Lapeire L, Hendrix A, Lambein K*, et al.* Cancer-associated adipose tissue promotes breast cancer progression by paracrine oncostatin M and Jak/STAT3 signaling. *Cancer Res* 2014; **74**: 6806-6819.
25. Reid J, Zamuner S, Edwards K*, et al.* Targeting Oncostatin M in the Target Tissue: Assessment of in-Vivo Affinity and Target Engagement of an Anti-OSM Monoclonal Antibody By Combining Blood and Skin Blister Fluid Data. *Arthritis Rheumatol* 2016; **68**: ACR/ARHP Annual Meeting Abstract Supplement.
26. Zijlstra A, Mellor R, Panzarella G*, et al.* A quantitative analysis of rate-limiting steps in the metastatic cascade using human-specific real-time polymerase chain reaction. *Cancer Res* 2002; **62**: 7083-7092.
27. Scotto L, Narayan G, Nandula SV*, et al.* Integrative genomics analysis of chromosome 5p gain in cervical cancer reveals target over-expressed genes, including Drosha. *Mol Cancer* 2008; **7**: 58.
28. Sticht C, Freier K, Knopfle K*, et al.* Activation of MAP kinase signalling through ERK5 but not ERK1 expression is associated with lymph node metastases in oral squamous cell carcinoma (OSCC). *Neoplasia* 2008; **10**: 462-470.
29. Estilo CL, P Oc, Talbot S*, et al.* Oral tongue cancer gene expression profiling: Identification of novel potential prognosticators by oligonucleotide microarray analysis. *BMC Cancer* 2009; **9**: 11.
30. Micci F, Panagopoulos I, Haugom L*, et al.* Genomic aberration patterns and expression profiles of squamous cell carcinomas of the vulva. *Genes Chromosomes Cancer* 2013; **52**: 551-563.
31. Hudson LG, Gale JM, Padilla RS*, et al.* Microarray analysis of cutaneous squamous cell carcinomas reveals enhanced expression of epidermal differentiation complex genes. *Mol Carcinog* 2010; **49**: 619-629.
32. Rheinwald JG, Beckett MA. Tumorigenic keratinocyte lines requiring anchorage and fibroblast support cultured from human squamous cell carcinomas. *Cancer Res* 1981; **41**: 1657-1663.
33. Hayes TF, Benaich N, Goldie SJ*, et al.* Integrative genomic and functional analysis of human oral squamous cell carcinoma cell lines reveals synergistic effects of FAT1 and CASP8 inactivation. *Cancer Lett* 2016; **383**: 106-114.
34. Rusnak DW, Lackey K, Affleck K*, et al.* The effects of the novel, reversible epidermal growth factor receptor/ErbB-2 tyrosine kinase inhibitor, GW2016, on the growth of human normal and tumor-derived cell lines in vitro and in vivo. *Mol Cancer Ther* 2001; **1**: 85-94.
35. Groves IJ, Knight EL, Ang QY*, et al.* HPV16 oncogene expression levels during early cervical carcinogenesis are determined by the balance of epigenetic chromatin modifications at the integrated virus genome. *Oncogene* 2016; **35**: 4773-4786.

Table 1. Correlations between levels of *OSMR* and those of *OSM, STAT3, EGFR, VEGFA* and *TGM2* in clinical samples of cervical, head/neck and lung SCCs.

Linear regression analysis of expression levels of *OSMR* versus those of *OSM, STAT3, EGFR, VEGFA* and *TGM2* in cervical (n=251), head/neck (n=504) and lung (n=499) SCC samples from TCGA (r = correlation coefficient).

Gene	Cervical SCC n = 251		Head and Neck SCC n = 504		Lung SCC n = 499	
	p value	r	p value	r	p value	r
OSM	0.049	0.124	2.1×10^{-6}	0.199	2.6×10^{-4}	0.157
STAT3	2.6×10^{-13}	0.440	$< 1.0 \times 10^{-16}$	0.354	5.6×10^{-14}	0.316
EGFR	$< 1.0 \times 10^{-16}$	0.621	$< 1.0 \times 10^{-16}$	0.585	$< 1.0 \times 10^{-16}$	0.400
VEGFA	7.5×10^{-9}	0.332	2.5×10^{-6}	0.197	4.1×10^{-4}	0.152
TGM2	3.3×10^{-7}	0.315	6.3×10^{-8}	0.226	4.0×10^{-11}	0.279

Figure Legends

Figure 1. Analysis of signalling pathways downstream of OSMR activation in SCC cells.

(A) Western blots showing activation of the indicated proteins in cells with high (SW756) or low (ME180) levels of OSMR, treated for 15 min with OSM or vehicle (ctrl). The blot exposure times varied between the cell lines. (B) Densitometric quantification of the blots shown in panel A. Phospho-protein levels are related to total levels of the respective proteins, while total EGFR and STAT1 are related to β-tubulin. Changes in each cell line are referred to vehicle-treated cells. Accordingly, the graphs do not show the differences in baseline levels of each protein between the cell lines. (C-D) Western blots showing activation of STAT3 and ERK1/2 in ME180 (C) and MS751 (D) cells transfected with control or OSMR plasmid and treated with OSM for 15 min. The numbers below the blots indicate relative densitometric quantification of the corresponding phospho-protein levels, related to total levels of the respective proteins. The levels of *OSMR* transcript expression in ME180 and MS751 cells were determined by RT-qPCR (C-D, right). OSMR protein was not detected satisfactorily in ME180 cells. (E) Western Blots of the indicated proteins 30 min and 4 h following OSM pulse treatment (15 min) in SW756 cells transfected with siRNAs against OSMR, LIFR or non-targeting control (siNTC). Data are presented as mean ± SEM. Transcript quantification values are from three independent experiments. The Western blots show data from one representative experiment, out of two performed.

Figure 2. Expression of the pro-malignant target genes *VEGFA, SNAI1* and *TGM2* in SCC cells with high versus low levels of OSMR.

Each panel shows RT-qPCR analysis of mRNA levels in OSM-treated SCC cells, comparing: (A) Two cervical SCC cells with high OSMR expression (SW756 and CaSki) versus two with low OSMR expression (ME180 and MS751); (B) MS751 cells transfected with OSMR over-expressing plasmid versus those transfected with the corresponding control plasmid; (C, D) OSMR-high cervical (C) or

skin and head/neck (D) SCC cells transfected with the indicated siRNAs, versus the same cells treated with non-targeting siRNAs (siNTC). Cells were treated with OSM for 24 h (A, C) or 48 h (B, D) prior to analysis. All expression values were first referenced to PBS-treated cells, then compared between the respective experimental groups. Key: * $p < 0.05$, ** $p < 0.01$, *** $p < 0.001$. Data are presented as mean ± SEM (n=4 for A, n=3 for B-D).

Figure 3. Effect of JAK/STAT3 inhibition on OSM pro-malignant effects in SCC cells.

(A) Western blots showing the effects of small molecule inhibitors on activation of their target signalling pathways in SW756 cells treated with OSM for 30 min. (B-E) qRT-PCR analysis of *VEGFA*, *SNAI1* and *TGM2* mRNA levels in SCC cells, examining: (B) SW756 cells treated with OSM or vehicle (PBS) for 24h; (C) SW756 cells over-expressing OSM; (D, E) SW756, CaSki, OSC19 and HSC1 cells transduced with STAT3 siRNAs and treated with OSM for 48h, compared with cells treated with non-targeting siRNAs (siNTC) and OSM. (F) Quantification of invasion in SW756 cells pre-treated with STAT3 siRNAs or siNTC and treated with OSM or PBS for 48 h. (G-H) Lung colonization in NOD-SCID mice following tail vein injection of SW756 cells in the presence of STAT3 siRNAs or siNTC, treated with OSM or vehicle (PBS) for 48 h. Luminescence images from the end point of the experiment are shown in (G) and the time course quantification of thoracic bioluminescent signal in H). For all panels, *p<0.05, **p<0.01, ***p<0.001. Data are presented as mean ± SEM (n=3 for B-E; n=5 for F; n=6 per group for G-H. Panel A shows data from one representative western blot, out of two performed.

Figure 4. Induction of feed forward signalling loops by OSMR activation.

(A, B) Western blots showing: (A) biphasic STAT3 activation and SOCS3 expression in OSM-pulsed SW756 cells; and (B) inhibition of STAT3 re-activation in SW756 cells by GolgiSTOP, assessed 4h after a 15min OSM pulse. (C-D) Levels of OSM (C) and IL6 (D) secretion by SW756 at various time-points after a 15 min OSM pulse, compared with untreated (Ctrl) cells. E) RT-qPCR analysis of *OSM* mRNA

levels in SW756 pulsed with OSM for 15 min. (F) Levels of OSM secretion by ME180 and MS751 cells over-expressing OSMR, 4 h after a 15 min OSM pulse. (G) Western blots showing OSMR levels following OSM pulse treatment of SW756 and ME180 cells. (H) Densitometric quantification of the blots in G. Changes in each cell line refer to untreated SW756 cells. (I) RT-qPCR analysis of *OSMR* transcript levels in SW756 cells constitutively over-expressing OSM . J-K) Western blots showing STAT3 activation in SW756 cells treated with anti-OSM (0.25 μg/ml), anti-IL6 (0.5 μg/ml) or control antibodies (IgG) (J); and OSMR levels and STAT3 activation in SW756 cells treated with anti-OSM or control (IgG) antibodies (0.25 μg/ml) (K), following a 15 min OSM pulse. For all panels, ***p<0.001. Data are presented as mean ± SEM (n=3 for C, D and F; n=2 for E; n=4 for I). The Western blots (panels A, B, G, H, J and K) show data from one representative experiment, out of two performed.

Figure 5. Effect of neutralizing anti-OSM antibodies on the pro-malignant phenotype of OSMR over-expressing SCC cells.

(A, B) Inhibition of OSM induction of OSM:OSMR target genes by neutralizing anti-OSM antibody in SW756 (A) and CaSki (B). The range of antibody concentrations was 8 ng/ml to 1 μg/ml. Cells were pre-treated with antibody, then with OSM for 24h. (C-E) Effects on *in vitro* angiogenesis of conditioned medium from SW756 cells treated for 48 h with OSM or vehicle (PBS) after pre-treatment with anti-OSM or control (IgG) antibodies. VEGF and suramin were positive and negative controls, respectively. Panel C shows representative images (bars=100 μm), while measurements for total tubule length and number of junctions are in D and E, respectively. (F-G) Quantification of invasion of SW756 (F) and OSC19 (G) cells pre-treated with anti-OSM or control (IgG1) antibodies, then treated for 48 h with OSM or vehicle (PBS). (H-I) Lung colonization in NOD-SCID mice following tail vein injection of SW756 cells treated for 48 h with OSM or vehicle (PBS), following pre-treatment with anti-OSM or control (IgG) antibodies. Luminescence images from the end point of the experiment are shown in (H) and time-course quantification of thoracic bioluminescent signal in (I). For all panels, *p<0.05, **p<0.01, ***p<0.001. Data represent mean ± SEM (n=4 for A-B; n=3 for D-E;

n=5 for F-G; n=6 per group for H-I). Panel C shows representative pictures from one experiment, out of three performed.

SUPPLEMENTARY MATERIAL ONLINE

Supplementary materials and methods

Supplementary figure legends

Figure S1. OSMR copy number and expression in SCC cell lines

Figure S2. OSMR over-expression in SCC cells enhances responsiveness to OSM

Figure S3. JAK2 and STAT3 mediate the pro-malignant effects of OSM:OSMR interactions

Figure S4. OSM induces a feed-forward loop in SCC cells, which prolongs STAT3 activation

Figure S5. IL6R and LIFR are not over-expressed in SCCs from multiple sites

Figure S6. Anti-OSM neutralising antibody inhibits OSM:OSMR pro-malignant signalling in SCC cells

Figure S7. Correlations between levels of *OSMR* and multiple signalling and downstream genes in clinical samples of cervical SCCs

Table S1. SCC cell lines used and their culture conditions

Table S2. siRNA pools used for gene depletion

Table S3. Primers used for qPCR

Table S4. Antibodies used for Western blotting

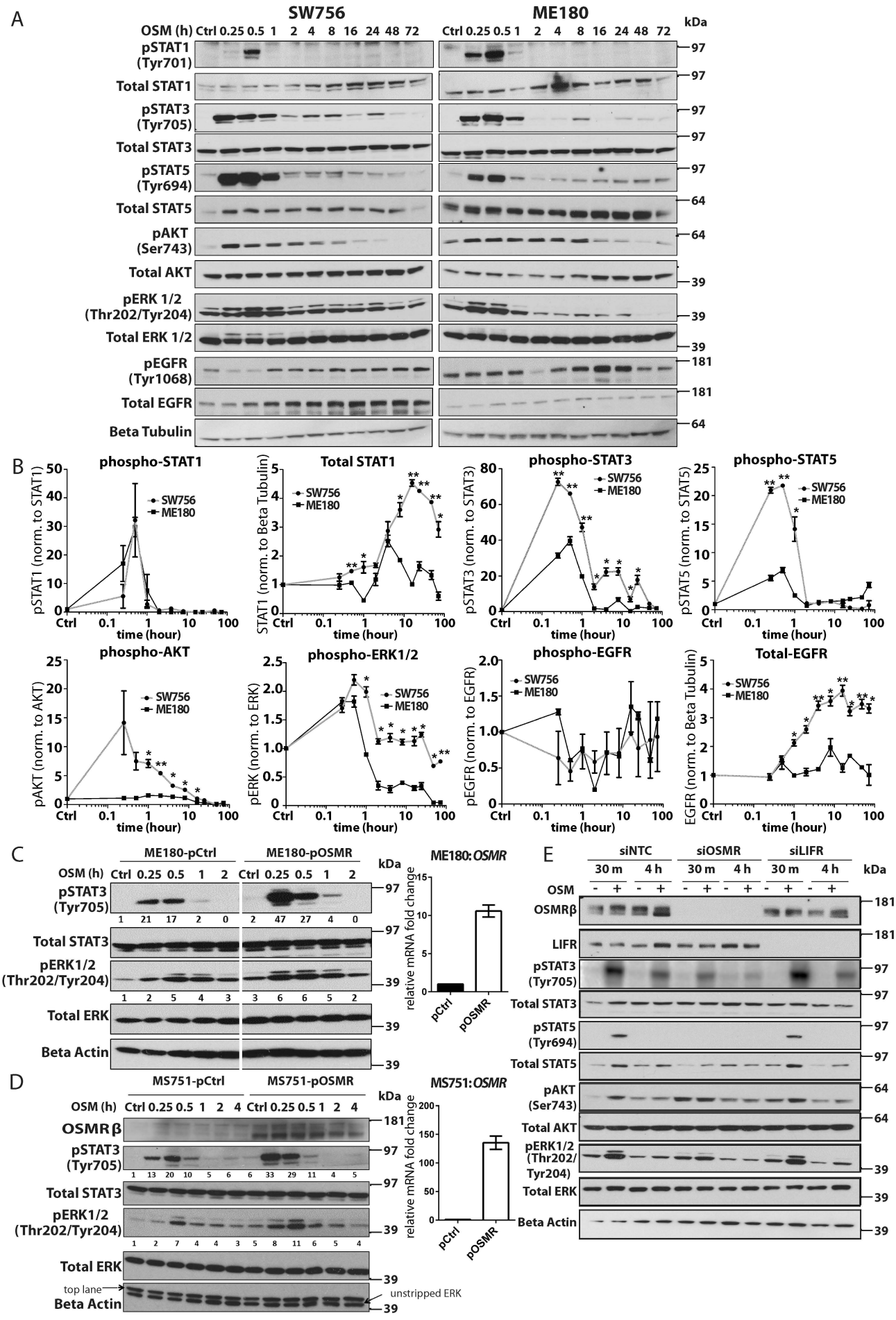
A
SW756
ME180
OSM (h) Ctrl 0.25 0.5 1 2 4 8 16 24 48 72
kDa
pSTAT1 (Tyr701)
Total STAT1
pSTAT3 (Tyr705)
Total STAT3
pSTAT5 (Tyr694)
Total STAT5
pAKT (Ser743)
Total AKT
pERK 1/2 (Thr202/Tyr204)
Total ERK 1/2
pEGFR (Tyr1068)
Total EGFR
Beta Tubulin
B
phospho-STAT1
pSTAT1 (norm. to STAT1)
Total STAT1
STAT1 (norm. to Beta Tubulin)
phospho-STAT3
pSTAT3 (norm. to STAT3)
phospho-STAT5
pSTAT5 (norm. to STAT5)
phospho-AKT
pAKT (norm. to AKT)
phospho-ERK1/2
pERK (norm. to ERK)
phospho-EGFR
pEGFR (norm. to EGFR)
Total-EGFR
EGFR (norm. to Beta Tubulin)
time (hour)
C
ME180-pCtrl
ME180-pOSMR
ME180:OSMR
relative mRNA fold change
pCtrl
pOSMR
D
MS751-pCtrl
MS751-pOSMR
MS751:OSMR
top lane
unstripped ERK
E
siNTC
siOSMR
siLIFR
30 m
4 h
OSM
OSMRβ
LIFR

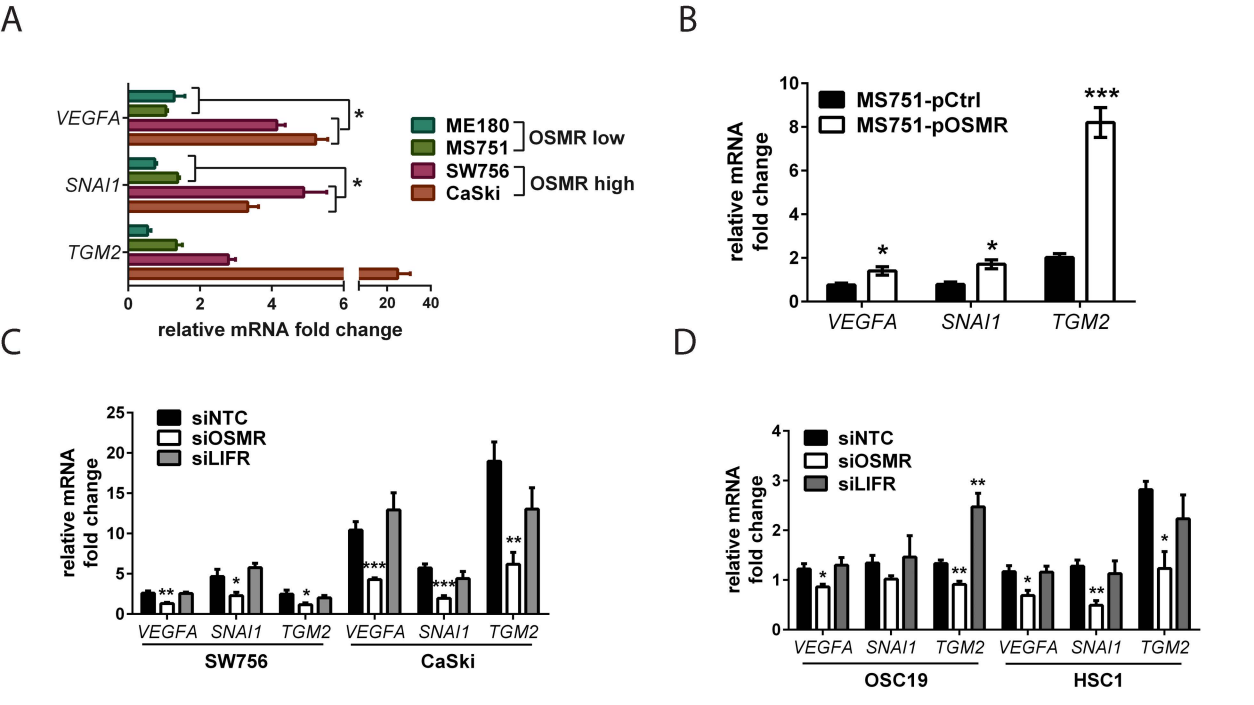
A
VEGFA
SNAI1
TGM2
*
*
ME180
MS751
SW756
CaSki
OSMR low
OSMR high
0
2
4
6
20
40
relative mRNA fold change
B
MS751-pCtrl
MS751-pOSMR
relative mRNA fold change
10
8
6
4
2
0
*
*
***
VEGFA
SNAI1
TGM2
C
siNTC
siOSMR
siLIFR
relative mRNA fold change
25
20
15
10
5
0
**
*
*
***
***
**
VEGFA
SNAI1
TGM2
VEGFA
SNAI1
TGM2
SW756
CaSki
D
siNTC
siOSMR
siLIFR
relative mRNA fold change
4
3
2
1
0
*
**
*
**
*
**
VEGFA
SNAI1
TGM2
VEGFA
SNAI1
TGM2
OSC19
HSC1

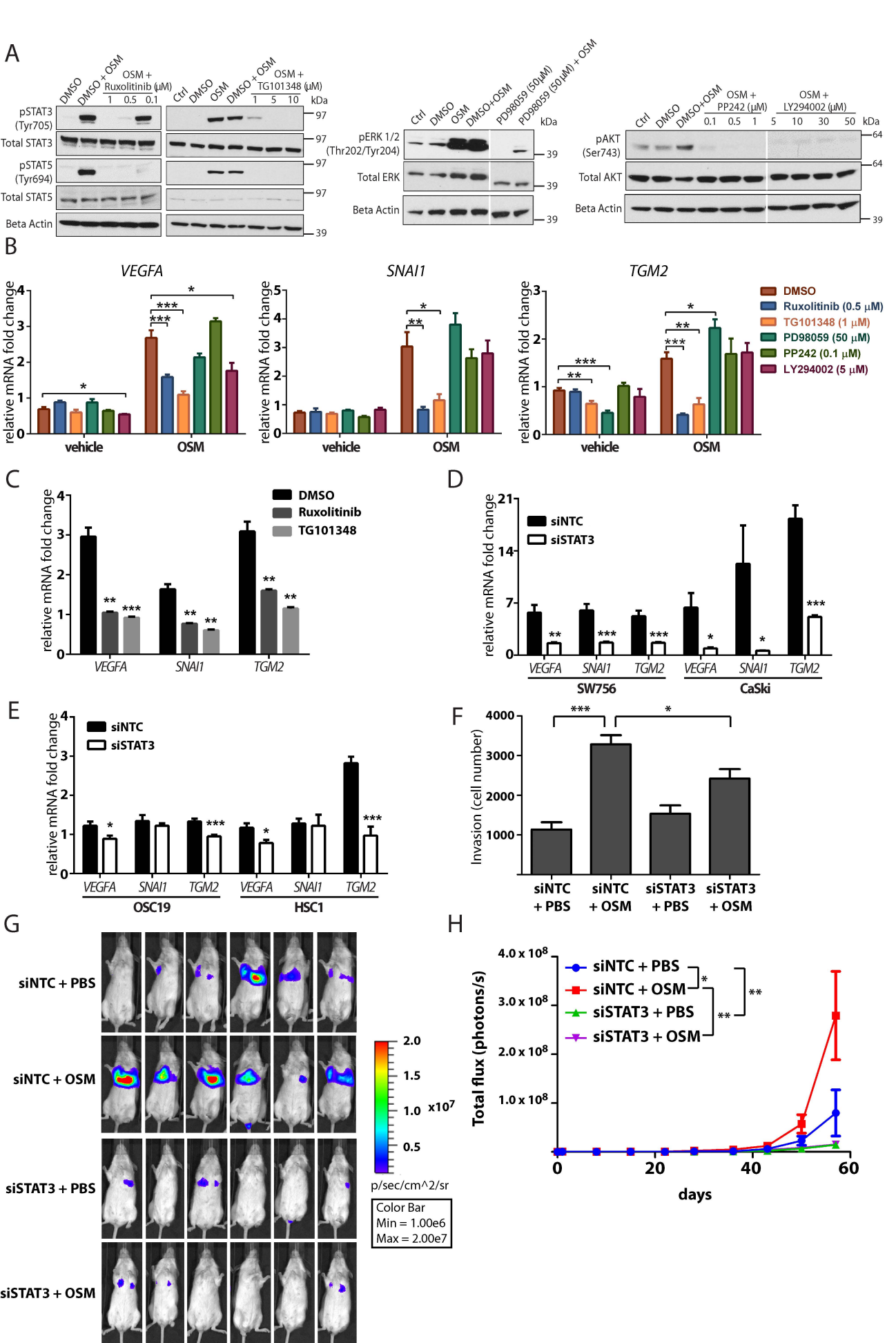
A
DMSO
DMSO + OSM
OSM + Ruxolitinib (μM)
1 0.5 0.1
Ctrl
DMSO
OSM
DMSO + OSM
OSM + TG101348 (μM)
1 5 10
kDa
pSTAT3 (Tyr705)
Total STAT3
pSTAT5 (Tyr694)
Total STAT5
Beta Actin
97
39
Ctrl
DMSO
OSM
DMSO+OSM
PD98059 (50μM)
PD98059 (50 μM) + OSM
pERK 1/2 (Thr202/Tyr204)
Total ERK
Beta Actin
OSM + PP242 (μM)
0.1 0.5 1
OSM + LY294002 (μM)
5 10 30 50
pAKT (Ser743)
Total AKT
64
B
VEGFA
SNAI1
TGM2
relative mRNA fold change
vehicle
OSM
DMSO
Ruxolitinib (0.5 μM)
TG101348 (1 μM)
PD98059 (50 μM)
PP242 (0.1 μM)
LY294002 (5 μM)
C
DMSO
Ruxolitinib
TG101348
D
siNTC
siSTAT3
SW756
CaSki
E
OSC19
HSC1
F
Invasion (cell number)
siNTC + PBS
siNTC + OSM
siSTAT3 + PBS
siSTAT3 + OSM
G
H
Total flux (photons/s)
days
p/sec/cm^2/sr
Color Bar
Min = 1.00e6
Max = 2.00e7

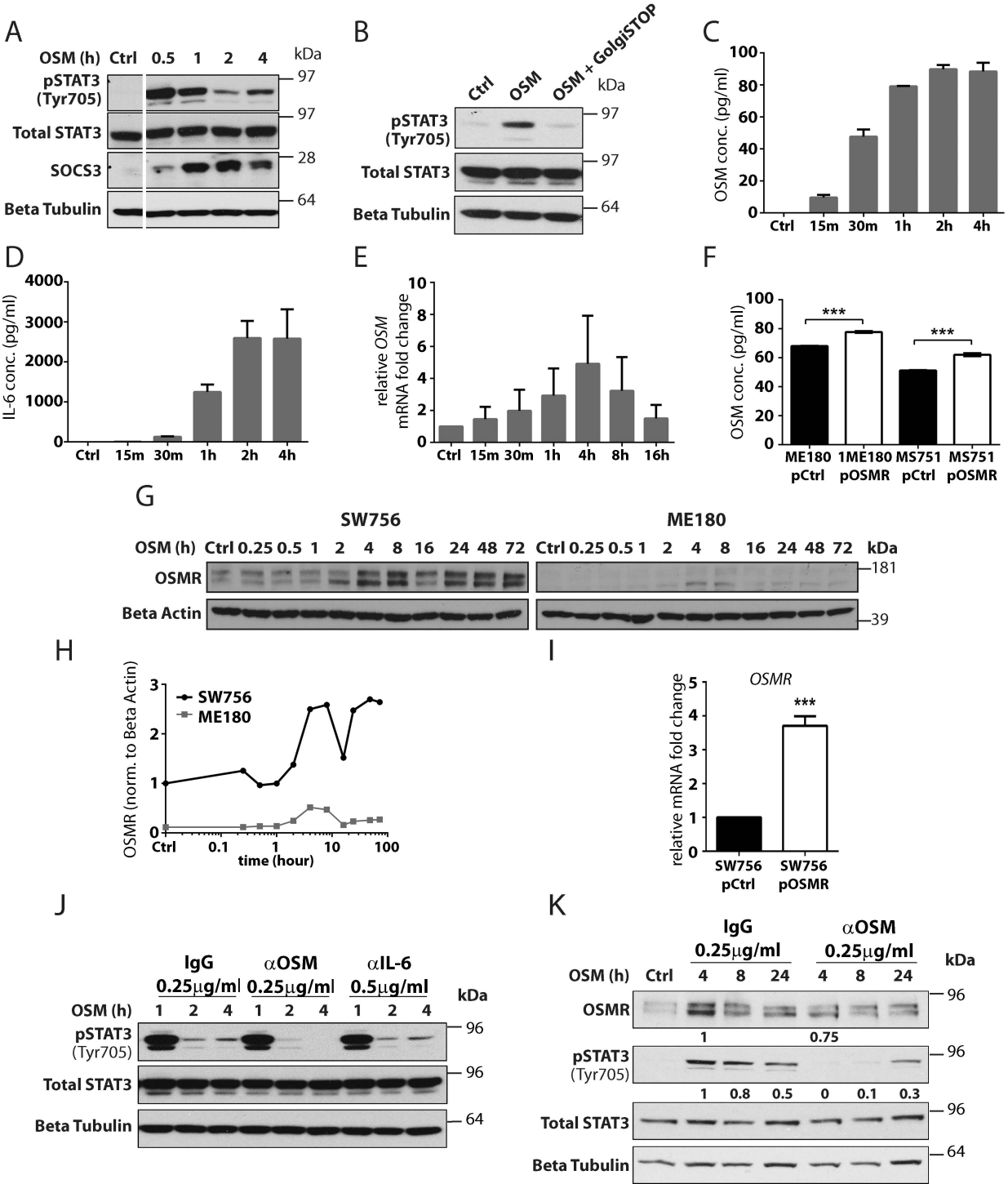
A
OSM (h) Ctrl 0.5 1 2 4 kDa
pSTAT3 (Tyr705)
Total STAT3
SOCS3
Beta Tubulin
97
97
28
64
B
Ctrl
OSM
OSM + GolgiSTOP
kDa
pSTAT3 (Tyr705)
Total STAT3
Beta Tubulin
97
97
64
C
OSM conc. (pg/ml)
Ctrl 15m 30m 1h 2h 4h
D
IL-6 conc. (pg/ml)
Ctrl 15m 30m 1h 2h 4h
E
relative OSM mRNA fold change
Ctrl 15m 30m 1h 4h 8h 16h
F
OSM conc. (pg/ml)
***
***
ME180 pCtrl
1ME180 pOSMR
MS751 pCtrl
MS751 pOSMR
G
SW756
ME180
OSM (h) Ctrl 0.25 0.5 1 2 4 8 16 24 48 72 Ctrl 0.25 0.5 1 2 4 8 16 24 48 72 kDa
OSMR
Beta Actin
181
39
H
OSMR (norm. to Beta Actin)
SW756
ME180
Ctrl 0.1 1 10 100
time (hour)
I
OSMR
***
relative mRNA fold change
SW756 pCtrl
SW756 pOSMR
J
IgG 0.25µg/ml
αOSM 0.25µg/ml
αIL-6 0.5µg/ml
kDa
OSM (h) 1 2 4 1 2 4 1 2 4
pSTAT3 (Tyr705)
Total STAT3
Beta Tubulin
96
96
64
K
IgG 0.25µg/ml
αOSM 0.25µg/ml
kDa
OSM (h) Ctrl 4 8 24 4 8 24
OSMR
1
0.75
96
pSTAT3 (Tyr705)
1 0.8 0.5 0 0.1 0.3
96
Total STAT3
96
Beta Tubulin
64

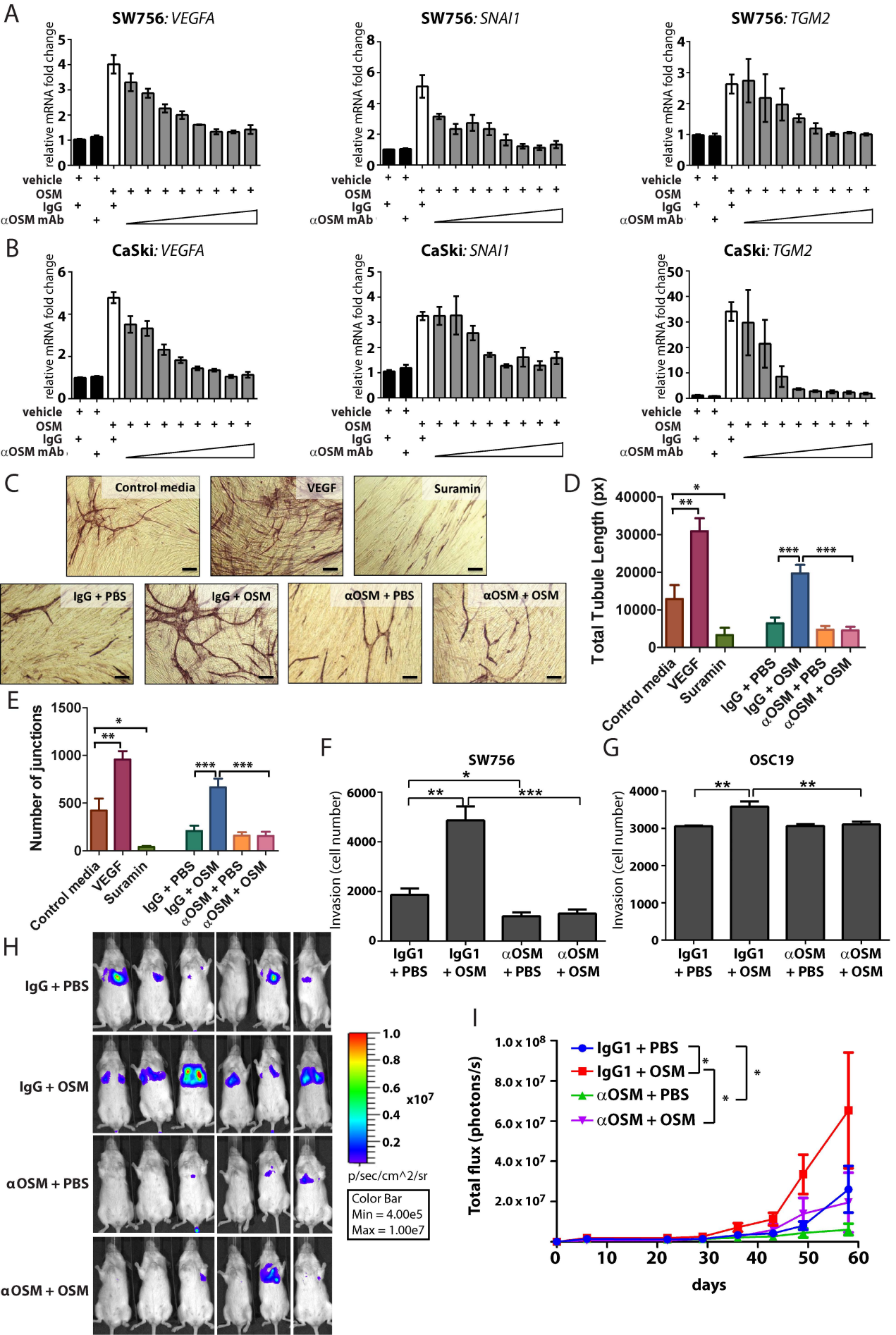
A
SW756: VEGFA
SW756: SNAI1
SW756: TGM2
relative mRNA fold change
vehicle
OSM
IgG
αOSM mAb
B
CaSki: VEGFA
CaSki: SNAI1
CaSki: TGM2
C
Control media
VEGF
Suramin
IgG + PBS
IgG + OSM
αOSM + PBS
αOSM + OSM
D
Total Tubule Length (px)
E
Number of junctions
F
SW756
Invasion (cell number)
IgG1 + PBS
IgG1 + OSM
αOSM + PBS
αOSM + OSM
G
OSC19
H
x10^7
p/sec/cm^2/sr
Color Bar
Min = 4.00e5
Max = 1.00e7
I
Total flux (photons/s)
days

Supplementary Materials and methods

Cell invasion assay

Invasion assays were performed in Boyden chambers, using the Cultrex basement membrane extract (BME) cell invasion assay (R&D Systems, Minneapolis, MN, USA). In brief, 0.5×10^5 SW756 or 0.25×10^5 OSC19 cells were subjected to different treatments (OSM stimulation, gene depletion or antibody treatment), starved for 24 h in serum-free medium, then seeded in the BME-coated upper chamber. The lower chamber was filled with medium supplemented with 10% FBS. After 24 hours, the cells that had invaded through the basement membrane were stained with Calcein-AM. Standard curves for each cell line were used to convert fluorescence values into cell numbers. All experiments were performed at least in triplicate and the mean values used to indicate invasion rates.

Angiogenesis assay

We measured endothelial tubule formation using co-cultures of human umbilical vein endothelial cells and primary human fibroblasts (V2a assay; Cellworks, San Jose, CA, USA). Forty-eight hours after cell seeding, the medium was replaced by conditioned medium from SW756 cells subjected to different treatments, or by control medium from untreated SW756 cells. Each type of medium was replaced every two days, for a duration of 14 days. Each conditioned medium sample was first clarified and concentrated using Amicon Ultra-4 Centrifugal Filter Units (Merck Millipore, Billerica, MA, USA), then re-suspended in V2a growth medium (Cellworks). Suramin (1 mM), an inhibitor of angiogenesis, and VEGFA (2 µg/ml) were used as negative and positive controls, respectively. To visualize the endothelial tubules, cells were fixed in cold ethanol (70%), stained with anti-human CD31 primary antibody and goat anti-mouse IgG-AP secondary antibody, then treated with BCIP/NBT substrate, according to the manufacturer's instructions for the V2A assay (all reagents from Cellworks). Total tubule length and the number of junctions formed were quantified using the AngioSys 2.0 Image Analysis Software (Cellworks).

Verification of In Vivo Imaging Software data

The data obtained by the In Vivo Imaging Software was confirmed using two independent methods: histology and RT-PCR of human DNA.

For histological analyses, haematoxylin and eosin stained histological lung sections were scanned at 20X using a Nanozoomer 2.0RS (C10730) (Hamamatsu Photonics K. K., Hamamatsu City, Japan). For determination of the area of lung affected by neoplastic aggregates, the scanned histological section was analysed using NDP.view2 viewing software (Hamamatsu Photonics K. K.). The 'freehand region' tool was used to measure the total scanned lung area, and to measure areas occupied by individual foci of neoplastic cells. The percentage of the analysed lung area affected by tumour was subsequently calculated from the measured values.

For quantification of human DNA in murine lungs, DNA was extracted from fixed lungs using the QIAamp DNA FFPE Tissue kit (Qiagen, Hilden, Germany) and quantitative real time PCR was performed as described in Materials and Methods by using primers for human Alu repetitive sequences (Forward primer: ACGCCTGTAATCCCAGCACTT; reverse primer: TCGCCCAGGCTGGAGTGCA) [26]. DNA ratios were normalized to human and mouse 45S ribosomal DNA (Forward primer: CGCGGTTCTATTTTGTTGGT ; reverse primer: CGGTCCAAGAATTTCACCTC).

Bioinformatics analysis of next generation sequencing data

Computational analysis and statistical testing were conducted using the R statistical programming language. Filtered and log2 normalized RNA expression data were downloaded from the Genome Data Analysis Centre Firehose database (run: stddata__2015_06_01) for each gene of interest from the cervical cancer (CESC), head and neck SCC (HNSCC) and lung SCC (LUSC) collections. Data downloads were performed using the FirebrowseR database access R package. Correlation testing

for associations between expressed genes was performed using the cor.test function in R to calculate the correlation coefficient (r) and test for significant deviation from no correlation. Plotting of correlation data was performed using the ggplot2 R package.

Statistics

Statistical analyses were performed using GraphPad Prism 6 software (GraphPad Software, La Jolla, CA, USA). For comparisons between groups we used Student's t-test and ANOVA, with *post hoc* analysis by the Student–Newman–Keuls' test. A p value of <0.05 was considered statistically significant. Data were presented as mean ± SEM. Time courses for the development of lung metastases *in vivo* were compared using linear mixed effects modelling, implemented in R via the lme4 package.

Supplementary Table S1. SCC cell lines used and their culture conditions

Cell line	Site of origin	Culture conditions	Reference / Supplier
CaSki	Cervix	GMEM (Sigma-Aldrich, St. Louis, USA)	ATCC (Middlesex, UK)
SW756	Cervix	GMEM	ATCC
ME180	Cervix	GMEM	ATCC
MS751	Cervix	GMEM	ATCC
SCC-25	Tongue	FAD (DMEM: Ham's F12, 3:1; Thermo Fisher Scientific, Waltham, MA, USA) + 3T3 irradiated feeders	Reinwald and Becket [32]
SCC-15	Tongue	FAD + 3T3 irradiated feeders	Reinwald and Becket [32]
OSC-19	Tongue	DMEM: Ham's F12, 1:1	JCRB cell bank
CAL 27	Tongue	DMEM	ATCC
FaDu	Pharynx	MEM (GE Healthcare, Little Chalfont, UK)	ATCC
Detroit 562	Pharynx	MEM	ATCC
SCC-4	Floor of mouth	FAD + 3T3 irradiated feeders	Reinwald and Becket [32]
SCC-12B.2	Skin	FAD + 3T3 irradiated feeders	Reinwald and Becket [32]
HSC-1	Skin	GMEM	JCRB cell bank
SCC-13	Skin	FAD + 1.36 ng/ml triiodo-L-thyronine, 5μg/ml insulin, 0.5 μg/ml hydrocortisone, 18 nM adenine and 10 ng/ml EGF	Reinwald and Becket [32]
SJG032	Mouth	FAD + 3T3 irradiated feeders	Hayes *et al.* [33]
HN5	Head and neck	DMEM	Rusnak *et al.* [34]
A-253	Submaxillary salivary gland	DMEM	ATCC

Key: ATCC - American Type Culture Collection, JCRB - Japanese Collection of Research Bioresources, DMEM - Dulbecco's Modified Eagle Medium, GMEM - Glasgow's Modified Eagle Medium, MEM - Minimum Essential Medium

Supplementary Table S2. siRNA pools used for gene depletion

Gene target	**ON-TARGETplus SMART pool**	**Sequence of individual duplexes**
Non-targeting control	D-001810-10-20	1: UGGUUUACAUGUCGACUAA 2: UGGUUUACAUGUUGUGUGA 3: UGGUUUACAUGUUUUCUGA 4: UGGUUUACAUGUUUUCCUA
LIFR	L-008017-01-0020	1: AGAACAAACCAAACGAUUA 2: GCAAUAUCUAGCAGCGUUA 3: GAGAGUAACAACACGGGAA 4: CGGAAACGAGAAUGGAUUA
OSMR	L-008050-00-0020	1: AGUCUUGGCUGAACGUUUA 2: UUUGAGAACUUGACCUAUA 3: CCUCGAUGCUGAUUCAUAU 4: AAUCUGAGCUCCCUUUGGA
STAT3	L-003544-00-0020	1: GAGAUUGACCAGCAGUAUA 2: CAACAUGUCAUUUGCUGAA 3: CCAACAAUCCCAAGAAUGU 4: CAACAGAUUGCCUGCAUUG

Supplementary Table S3. Primers used for qPCR

	Gene	Forward Primer (5' to 3')	Reverse Primer (5' to 3')	Reference / Supplier
Complementary DNA primers	*EGFR*	NM_005228	NM_005228	Sigma KiCqStart™ (Sigma, St. Louis, USA)
	HMBS	GGCAATGCGGCTGCAA	GGGTACCCACGCGAATCAC	Vandesompele *et al*. [21]
	LIFR	Hs_LIFR_1_SG	Hs_LIFR_1_SG	QuantiTect (QIAGEN, Crawley, UK)
	OSMR	Hs_OSMR_1_SG	Hs_OSMR_1_SG	QuantiTect (QIAGEN)
	RPL13A	CCTGGAGGAGAAGAGGAAAGAGA	TTGAGGACCTCTGTGTATTTGTCAA	Vandesompele *et al*. [21]
	SNAI1	TCGGAAGCCTAACTACAGCGA	AGATGAGCATTGGCAGCGAG	PrimerBank
	STAT1	NM_007315	NM_007315	Sigma KiCqStart™
	STAT3	Hs_STAT3_1_SG	Hs_STAT3_1_SG	QuantiTect (QIAGEN)
	STAT5A	NM_003152	NM_003152	Sigma KiCqStart™
	STAT5B	NM_012448	NM_012448	Sigma KiCqStart™
	STAT6	NM_001178078	NM_001178078	Sigma KiCqStart™
	TGM2	Hs_TGM2_1_SG	Hs_TGM2_1_SG	QuantiTect (QIAGEN)
	VEGFA	NM_001204384	NM_001204384	Sigma KiCqStart™

	YWHAZ	ACTTTTGGTACATTGTGGCTTCAA	CCGCCAGGACAAACCAGTAT	Vandesompele *et al*. [21]
Genomic DNA primers	*ACTB*prom	CTGATGCCACAATCACCCCT	GTAATGTATTAACTTCCTGGCCATT	Groves *et al*. [35]
	*GAPDH*prom	CGGCTACTAGCGGTTTTACG	AAGAAGATGCGGCTGACTGT	Groves *et al*. [35]
	*MYOG*prom	GGAGAAAGAAGGGGAATCACAT	GATAAATATAGCCAACGCCACA	Groves *et al*. [35]
	OSMR	GACAACTTCGCAGCCCATC	GTAGCCCAGCCAAGCAAAC	Own design

Supplementary Table S4. Antibodies used for Western blotting

Target	Antibody catalogue number	Supplier	Host species	Dilution
AKT	**9272**	Cell Signaling Technology (Danvers, MA, USA)	rabbit	1 : 1000
EGFR	**ab52894**	Abcam (Cambridge, UK)	rabbit	1 : 100000
ERK	**610124**	BD Biosciences (San Jose, CA, USA)	mouse	1 : 1000
LIFR	**sc-659**	Santa Cruz Biotechnology (Dallas, TX, USA)	rabbit	1 : 1000
OSMR β	**sc-30010**	Santa Cruz Biotechnology	rabbit	1 : 500
Phospho-AKT (Ser473)	**9271**	Cell Signaling Technology	rabbit	1 : 1000
Phospho-EGFR (Tyr1068)	**ab32430**	Abcam	rabbit	1 : 10000
Phospho-p44/42 MAPK (Erk1/2) (Thr202/Tyr204)	**9101**	Cell Signaling Technology	rabbit	1 : 1000
Phospho-STAT1 (Tyr701)	**7649**	Cell Signaling Technology	rabbit	1 : 1000
Phospho-STAT3 (Tyr705)	**9145**	Cell Signaling Technology	rabbit	1 : 2000
Phospho-STAT5 (Tyr694)	**9359**	Cell Signaling Technology	rabbit	1 : 1000
SOCS3	**sc-7009**	Santa Cruz Biotechnology	goat	1 : 1000

STAT1	**9172**	Cell Signaling Technology	rabbit	1 : 1000
STAT3	**9139**	Cell Signaling Technology	mouse	1 : 1000
STAT5	**610191**	BD Biosciences	mouse	1 : 1000
β actin	**ab6276**	Abcam	mouse	1 : 150000
β tubulin	**ab6046**	Abcam	rabbit	1 : 10000
Rabbit	**P044801**	Dako (Glostrup, Denmark)	goat	1 : 2000
Mouse	**P044701**	Dako	goat	1 : 2000
Goat	**P044901**	Dako	rabbit	1 : 1000

Supplementary Figure legends

Figure S1. OSMR copy number and expression in SCC cell lines

(A-F) Quantification of OSMR relative gene copy number (A), mRNA (B) and protein (C-F) levels in a panel of 17 SCC cell lines from different anatomical sites, plus three primary cultures of basal-type normal cervical squamous cells (NCx). *OSMR* relative gene copy number (A) was determined by q-PCR, referenced to normal cervical cells with one copy of the *OSMR* gene per haploid genome (NCx6). *OSMR* mRNA expression (B) was also determined by RT-qPCR, referenced to CaSki cells, which had previously been shown to over-express OSMR at 3.4-fold greater levels than a pool of four independent cultures of basal-type normal cervical squamous cells [8]. Protein levels were determined by Western blotting (C-F), with densitometric quantification using Ponceau staining (C) or beta-actin (E) as loading controls and CaSki as the reference sample. Data in panels A, B, D and F are presented as mean ± SEM (n=3). Western blots (panels C and E) show data from one representative experiment, out of two performed. (G, H) Correlation testing for associations between OSMR protein levels across the 17 SCC cells and *OSMR* relative gene copy number (G) or mRNA expression (H). R^2 = coefficient of determination.

Figure S2. OSMR over-expression in SCC cells enhances responsiveness to OSM

(A) Flowchart summary of the OSM pulse procedure. (B) Western Blots showing activation of the indicated proteins in cells with high (SW756) or low (ME180) levels of OSMR, at various time points following a 15 min pulse with OSM or vehicle (ctrl). (C) RT-qPCR analysis of *EGFR* mRNA levels in SW756 cells treated with OSM for 24 and 48 hours. (D-F) Western Blots showing rapid activation of STAT3 (D-F) and ERK (F) by OSM (continuous treatment at 10 ng/ml) in OSC19 (D), HSC1 (E) and high- and low- OSMR cervical SCC cells (F). (G) Western Blots showing activation of STAT3 after 30 min of 100 ng/ml LIF in SW756 cells. (H) Western Blots of the indicated proteins 30min and 4h following OSM pulse treatment (15 min) in ME180 cells transfected with siRNAs against OSMR, LIFR or non-

targeting control (siNTC). (I) RT-qPCR analysis of mRNA levels of *OSMR* and *LIFR* in ME180 cells transfected with siOSMR or siLIFR. J-K) RT-qPCR analysis *of VEGFA, SNAI1* and *TGM2* mRNA levels in OSC19 (J) and HSC1 (K) cells treated with OSM for 48 h, compared with PBS-treated controls. L-M) RT-qPCR analysis of mRNA levels of *OSM*R (L) and *LIFR* (M) in SW756, CaSki, OSC19 and HSC1 cells transfected with siOSMR (L) or siLIFR (M). Key: siNTC: non-targeting control siRNAs; KD: knock-down. ** $p < 0.01$, *** $p < 0.001$. Data are presented as mean ± SEM (n=2 for C, n=4 for J-K; n=3 for I, L-M). Western blots (panels B, D-H) show data from one representative experiment, out of two performed.

Supplementary Figure S3. JAK2 and STAT3 mediate the pro-malignant effects of OSM:OSMR interactions

(A-E) SW756 cell growth curves in the presence of different small molecule inhibitors at the indicated concentrations. Growth was determined by MTT assay and normalised to levels at day 1. F) ELISA measurements of OSM secretion by SW756 cells transfected with control or OSM over-expressing plasmid. (G) RT-qPCR analysis of *VEGFA, SNAI1* and *TGM2* mRNA levels in SW756 cells transfected with control (pCtrl) or OSM over-expressing (pOSM) plasmid. (H-I) Western Blots showing lack of specific STAT3 inhibition in SW756 by the small molecule inhibitors S3i-201 (H) and Stattic (I) at the indicated concentrations. The white line in H indicates non-contiguous lanes from the same membrane. (J) RT-qPCR analysis showing *STAT3, STAT1, STAT5A, STAT5B* and *STAT6* mRNA levels after SW756 cell transfection with siSTAT3, compared with cells treated with non-targeting control siRNAs. K-N) RT-qPCR analysis of *STAT3* mRNA levels in SW756, CaSki, OSC19 and HSC1 cells transfected with non-targeting control siRNAs (siNTC) or siSTAT3. O) RT-qPCR analysis of *VEGFA, SNAI1* and *TGM2* mRNA levels in SW756 cells pre-treated with control (siNTC) or STAT3 siRNAs, then treated with vehicle (PBS) or OSM and subsequently used in the *in vivo* experiment shown in Figure 3 and in panels P, Q and R of this Figure. (P, Q) Luminescent images (P) and quantification of the thoracic bioluminescent signal (Q) of NOD-SCID mice 1 h post tail-vein injection of SW756 cells pre-

treated with control (NTC) or STAT3 siRNAs, followed by OSM or PBS treatment, in the *in vivo* experiment shown in Figure 3. There is even delivery of SW756 cells across the various groups. (R) Representative images of lung tissue at the end point of the *in vivo* experiment shown in Figure 3G, H. Scale bar: 500 μm. * $p < 0.05$, ** $p < 0.01$, *** $p < 0.001$. Data are presented as mean ± SEM (n=3 for A-F; n=5 for G; n=2 for J; n=6 per group for P-R). Western blots (panels H and I) show data from one representative experiment, out of two performed. Key: KD: knock-down; siNTC: non-targeting control siRNAs.

Figure S4. OSM induces a feed-forward loop in SCC cells, which prolongs STAT3 activation

(A) Western blots showing STAT3 activation in SW756 cells treated with anti-OSM (1 μg/ml), anti-IL6 (2.5 μg/ml) or control (IgG) (1 μg/ml) antibodies, following a 15 min OSM pulse. (B) Western blot showing lack of activation of STAT3 after 30 min by IL6 in SW756 cells. (C) RT-qPCR analysis of *VEGFA*, *SNAI1* and *TGM2* mRNA levels in SW756 cells treated with IL6 (100 ng/ml) for 48 h, compared with PBS-treated controls. (D) RT-qPCR analysis of *IL6R* mRNA levels in SW756 cells treated with OSM (10 ng/ml), compared with PBS-treated controls. E) Western Blots showing STAT3 activation in SW756 cells treated with PBS, anti-OSM or control (IgG) antibodies (0.25 μg/ml) for 24 h. Data are presented as mean ± SEM (n=3 for C-D). Western blots (panels A-B and E) show data from one representative experiment, out of two performed.

Figure S5. IL6R and LIFR are not over-expressed in SCCs from multiple sites

Transcript levels of *IL6R* (left column) and *LIFR* (right column) in SCC versus normal tissue from multiple anatomical sites. Data were derived from published gene expression profiles of cervix [27] (A,B), oral cavity [28] (C,D), tongue [29] (E,F), vulva [30] (G,H) and skin [31] (I,J). The number of samples analysed is indicated in each panel.

Figure S6. Anti-OSM neutralising antibody inhibits OSM:OSMR pro-malignant signalling in SCC cells.

(A) RT-qPCR analysis of *VEGFA, SNAI1* and *TGM2* mRNA levels in SW756 cells pre-treated with control IgG or antibody against OSM, followed by 48 h treatment with OSM or PBS, and subsequently used in the *in vivo* experiment shown in Figure 5 and this Figure. (B, C) Luminescent images (B) and quantification of the thoracic bioluminescent signal (C) of NOD-SCID mice 1 h post tail-vein injection of SW756 cells pre-treated with control IgG or antibody against OSM, followed by 48 h treatment with OSM or PBS, in the *in vivo* experiment shown in Figure 5. There is even delivery of SW756 cells across the various groups. (D) Representative images of lung tissue (left) and whole lungs (right) at the end point of the *in vivo* experiment shown in Figure 5H-I. Scale bars: 500 μm (left) and 1 mm (right). (E) Time-course quantification of thoracic bioluminescent signal in NOD-SCID mice following tail vein injection of SW756 cells treated for 48 h with vehicle (PBS), following pre-treatment with anti-OSM or control (IgG) antibodies, from the *in vivo* experiment shown in Figure 5. The Figure has been extracted from Figure 5I, for clarity. Data are presented as mean ± SEM (n=6 per group for A-E). (F, G) Linear regression analysis of thoracic bioluminescent signal for each mouse at the end of the experiment, versus quantification of lung colonization by histological analysis (F, n=7) and qPCR quantification of human DNA (G, n=24). In each plot, Spearman correlation coefficient (r) and p values are shown.

Figure S7. Correlations between levels of *OSMR* and multiple signalling and downstream genes in clinical samples of cervical SCCs

Linear regression analysis of expression levels of *OSMR* versus those of *OSM*, *STAT3*, *EGFR*, *VEGFA* and *TGM2* in cervical SCC samples from TCGA (n=251). For each gene, correlation coefficient (r) and p values are shown.

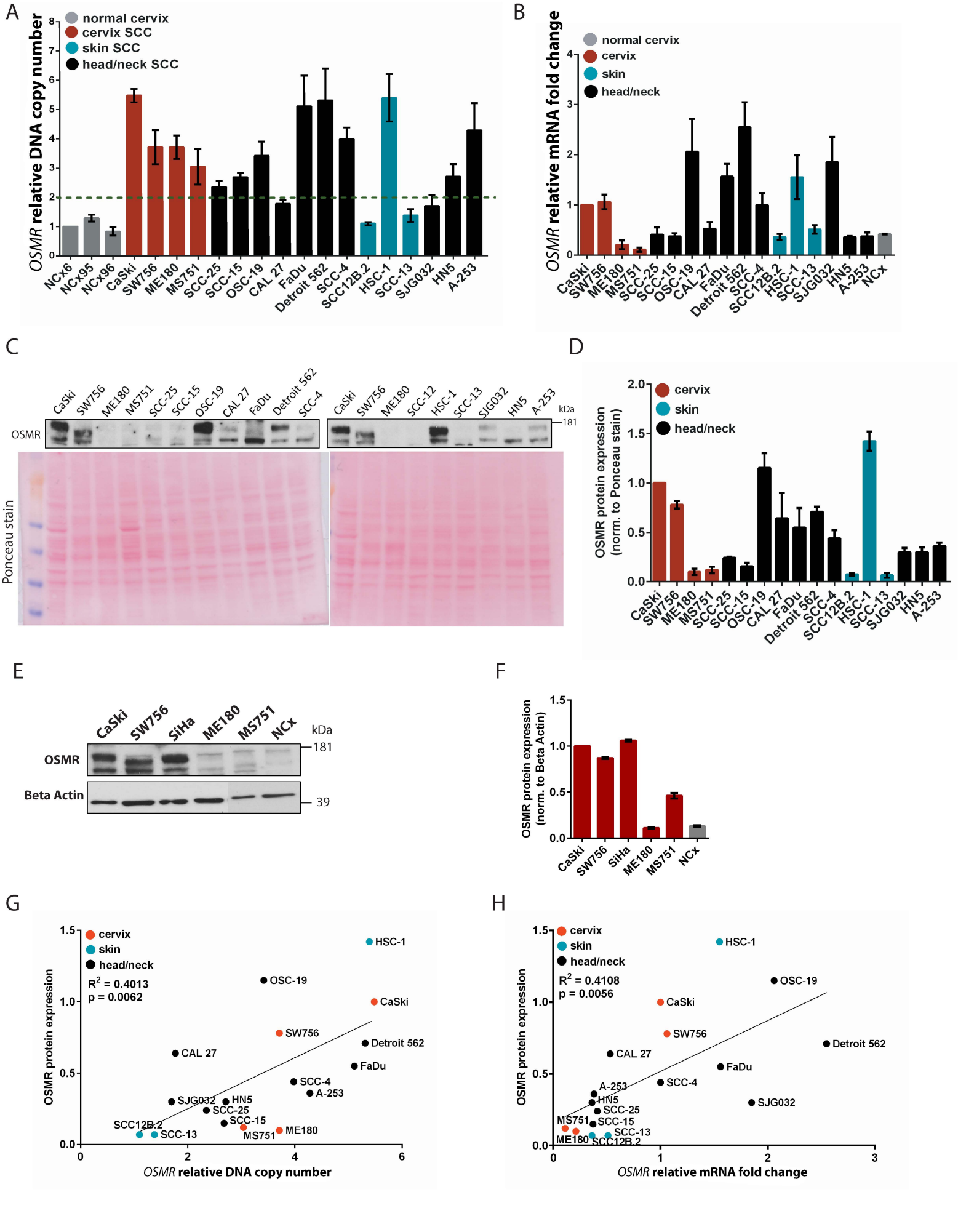

Supplementary Figure S1

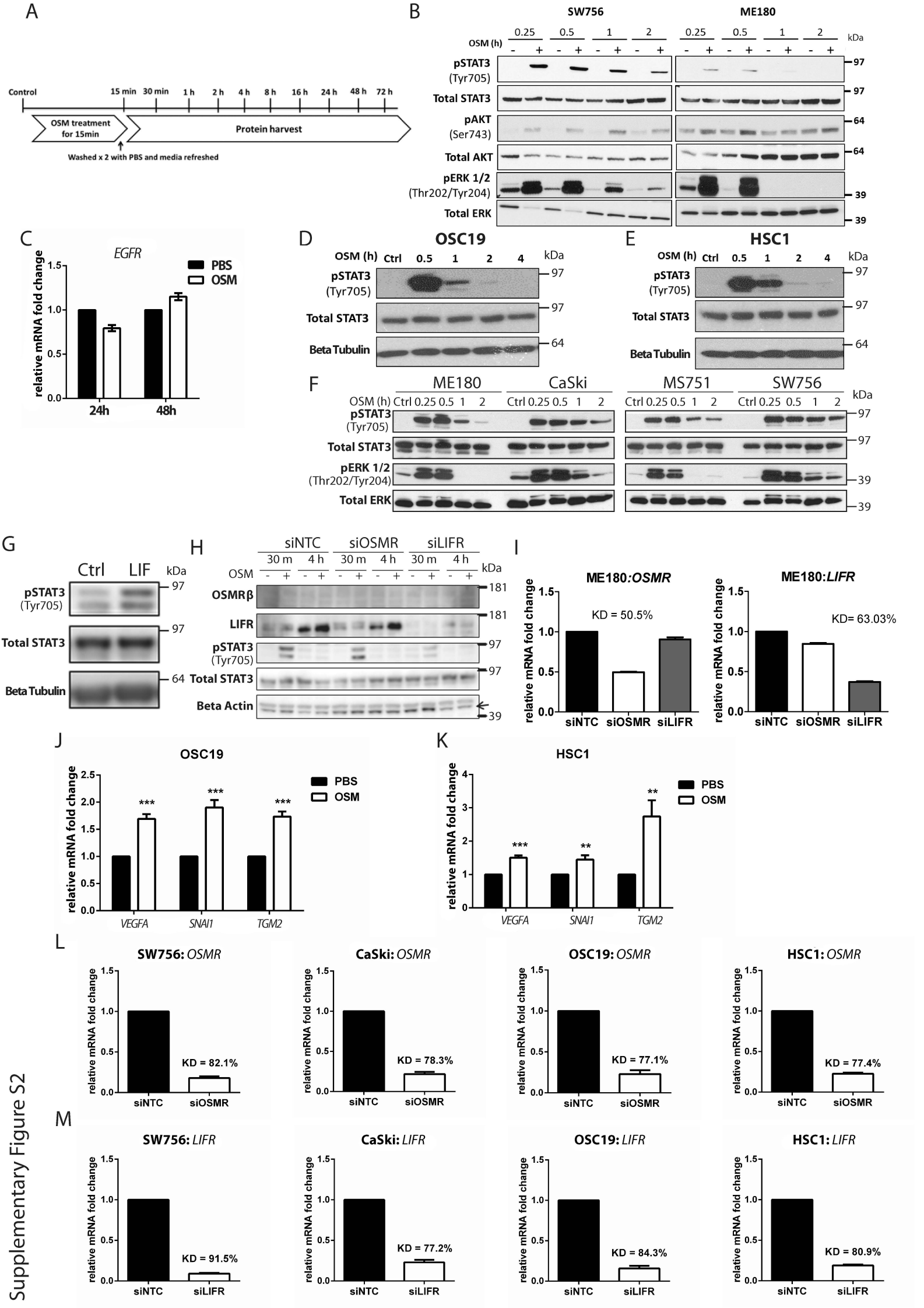

Supplementary Figure S2

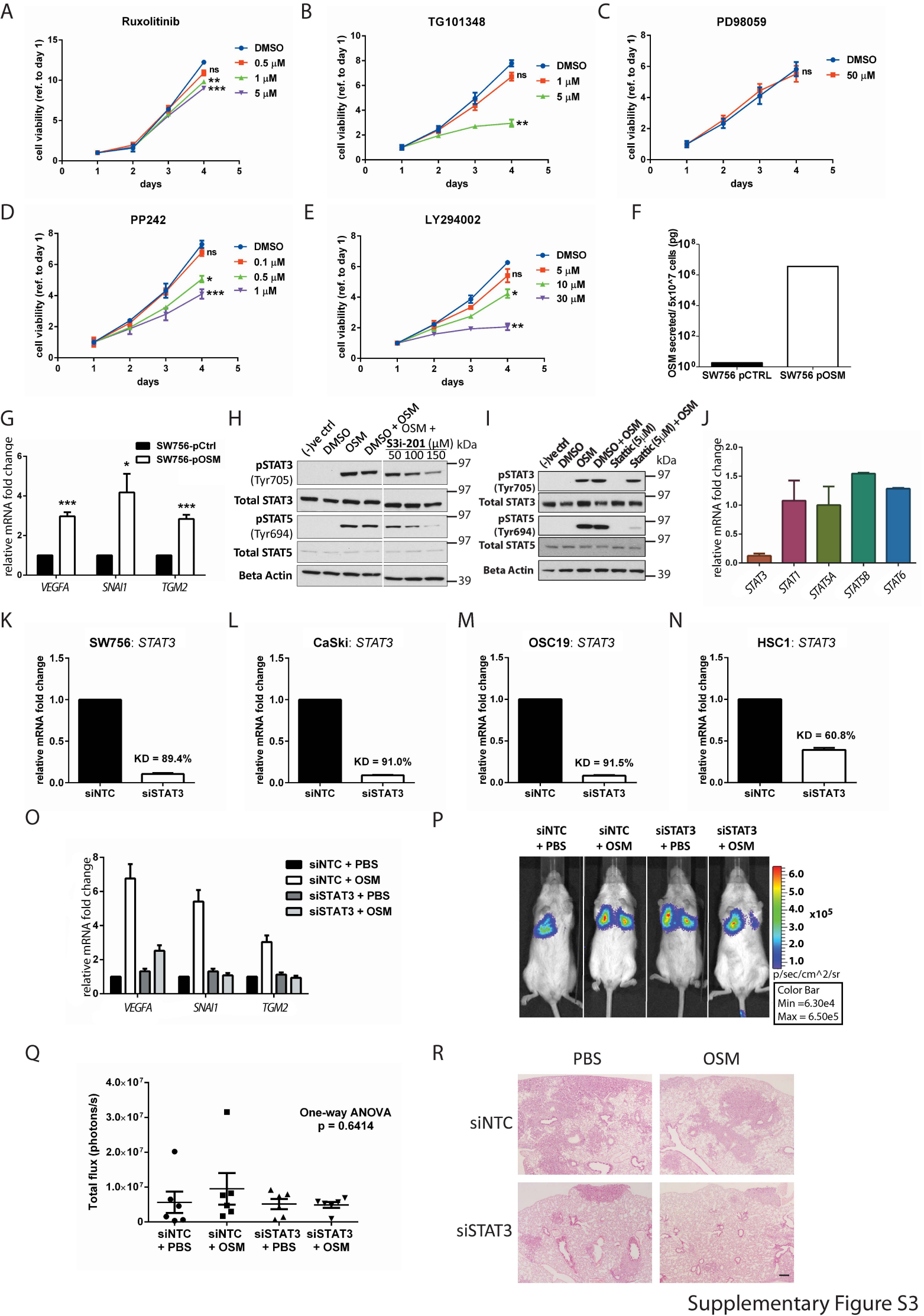

Supplementary Figure S3

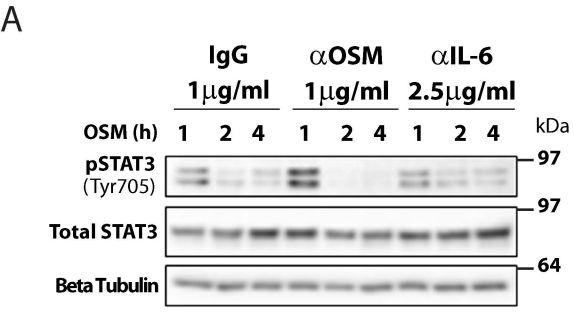

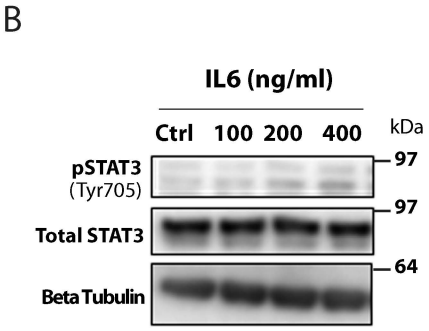

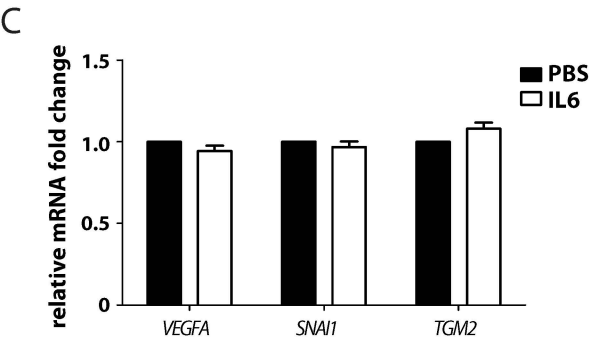

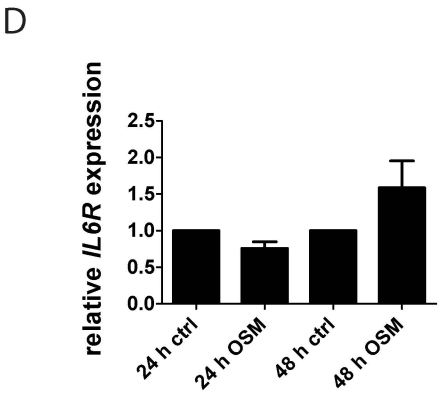

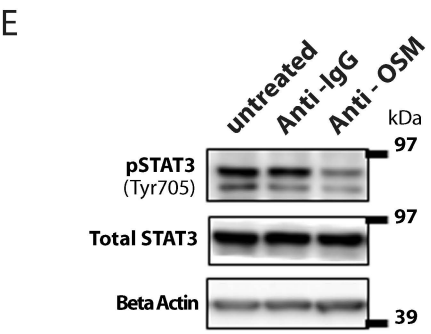

Supplementary Figure S4

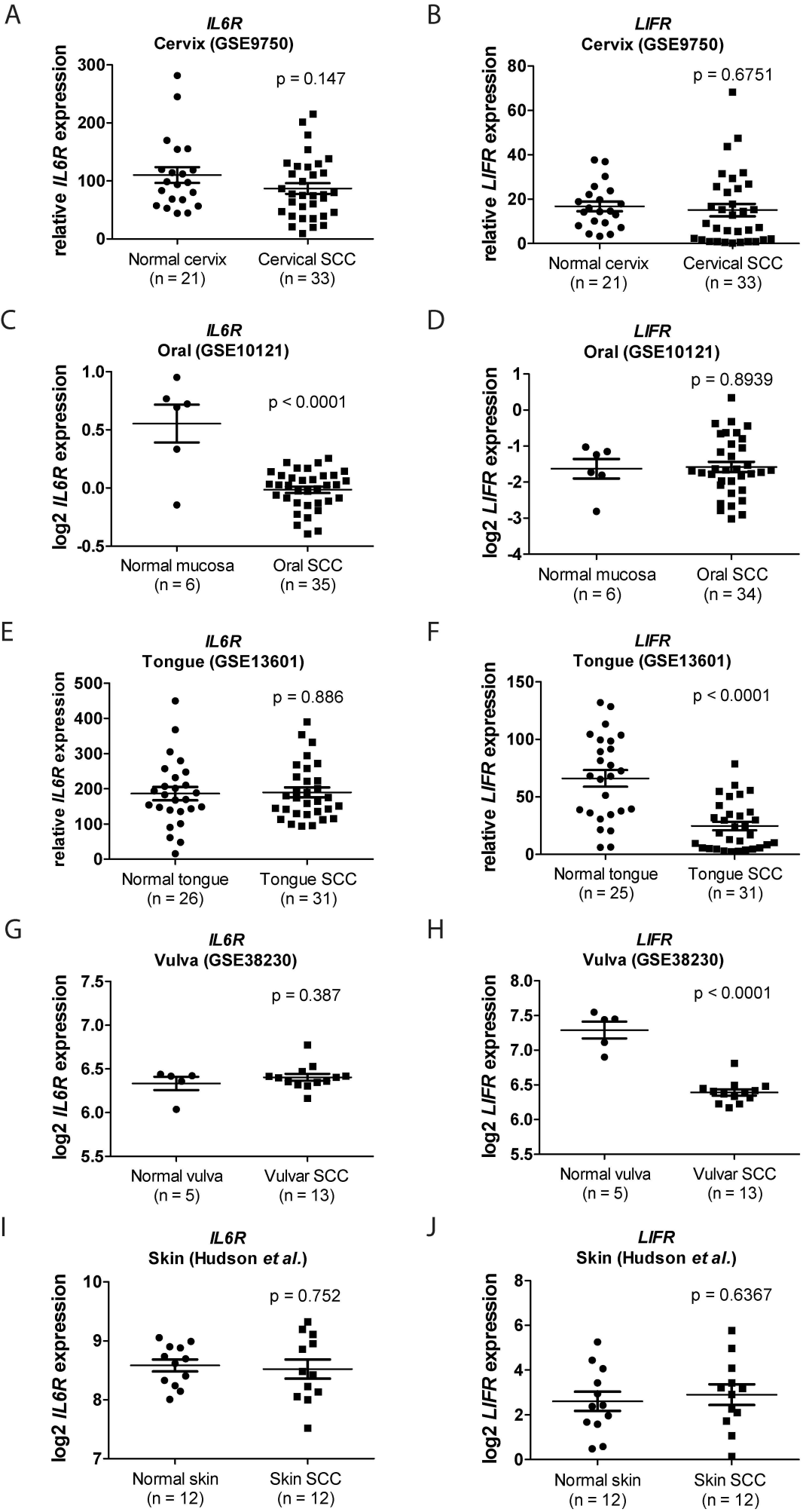

Supplementary Figure S5

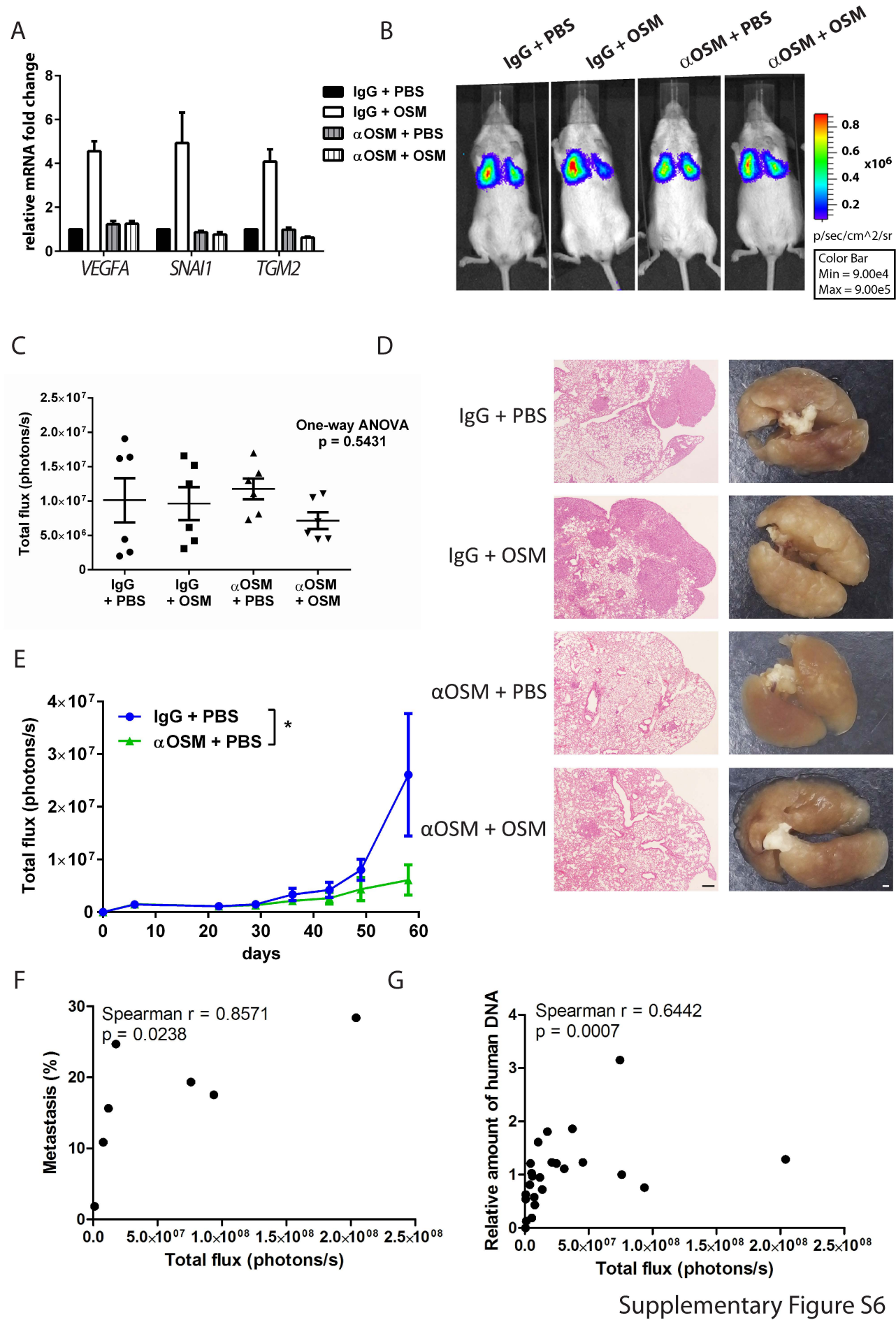

Supplementary Figure S6

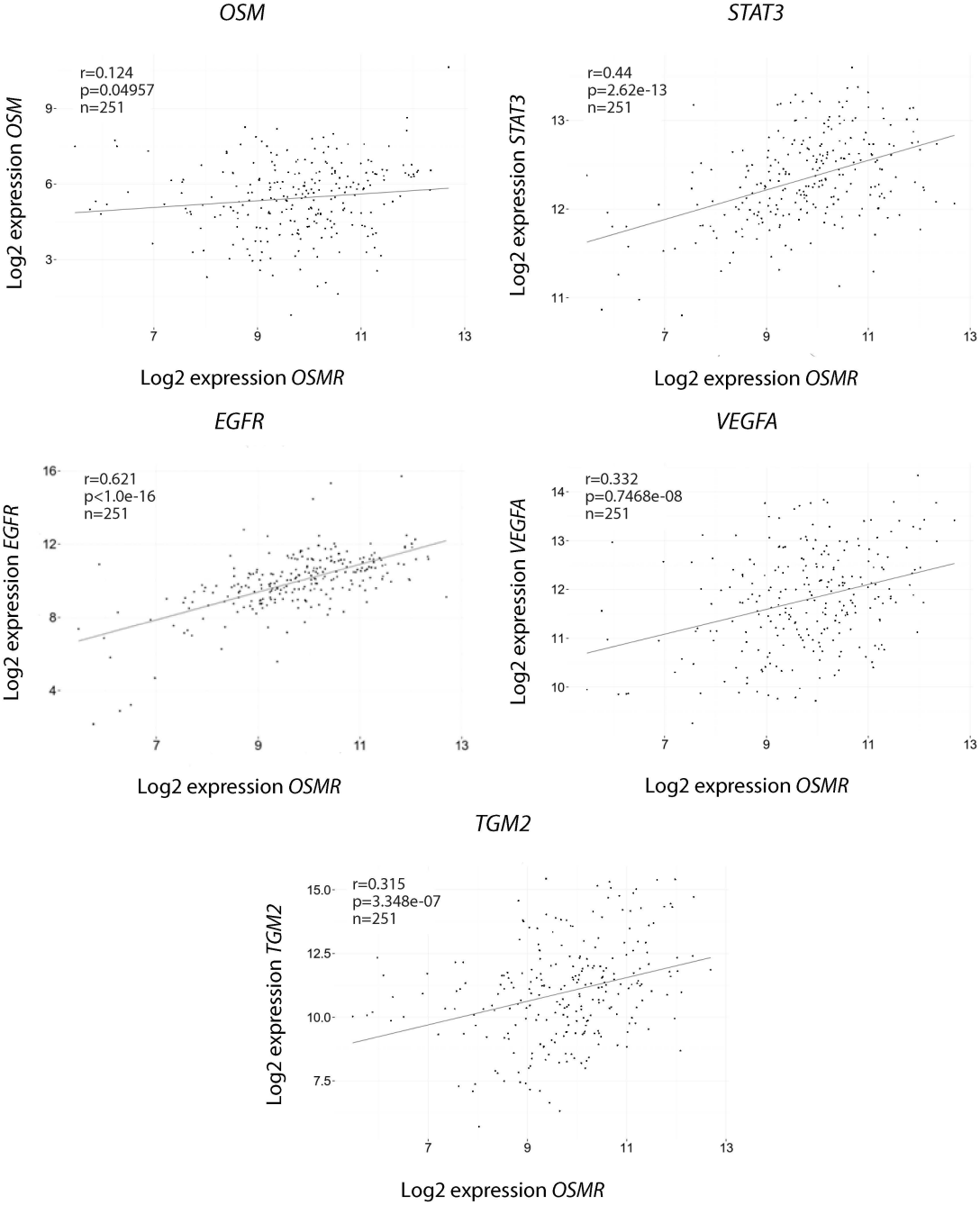

Supplementary Figure S7